



Natural Resources
Canada

Ressources naturelles
Canada

**GEOLOGICAL SURVEY OF CANADA
OPEN FILE 8585**

**U-Pb zircon geochronology of Archean greenstone belts
(Mary River Group) and surrounding Archean to
Paleoproterozoic rocks, northern Baffin Island, Nunavut**

**D.R. Skipton, N. Wodicka, V. McNicoll, B.M. Saumur,
M.R. St-Onge, and M.D. Young**

2019

Canada



**GEOLOGICAL SURVEY OF CANADA
OPEN FILE 8585**

**U-Pb zircon geochronology of Archean greenstone belts
(Mary River Group) and surrounding Archean to
Paleoproterozoic rocks, northern Baffin Island, Nunavut**

**D.R. Skipton^{1,2}, N. Wodicka¹, V. McNicoll¹, B.M. Saumur³, M.R. St-Onge¹,
and M.D. Young⁴**

¹ Geological Survey of Canada, 601 Booth Street, Ottawa, Ontario K1A 0E8

² Yukon Geological Survey, Department of Energy, Mines and Resources, Government of Yukon, 91807
Alaska Highway, Whitehorse, Yukon Y1A 2C6

³ Département des sciences de la Terre et de l'atmosphère, Université du Québec à Montréal, 201 avenue du
Président-Kennedy, Montréal, Québec H2X 3Y7

⁴ Department of Earth Sciences, Dalhousie University, 1355 Oxford Street, Halifax, Nova Scotia B3H 4R2

2019

© Her Majesty the Queen in Right of Canada, as represented by the Minister of Natural Resources, 2019

Information contained in this publication or product may be reproduced, in part or in whole, and by any means, for personal or public non-commercial purposes, without charge or further permission, unless otherwise specified.

You are asked to:

- exercise due diligence in ensuring the accuracy of the materials reproduced;
 - indicate the complete title of the materials reproduced, and the name of the author organization; and
 - indicate that the reproduction is a copy of an official work that is published by Natural Resources Canada (NRCan) and that the reproduction has not been produced in affiliation with, or with the endorsement of, NRCan.
- Commercial reproduction and distribution is prohibited except with written permission from NRCan. For more information, contact NRCan at nrcan.copyrightdroitdauteur.nrcan@canada.ca.

Permanent link: <https://doi.org/10.4095/314938>

This publication is available for free download through GEOSCAN (<https://geoscan.nrcan.gc.ca/>).

Recommended citation

Skipton, D.R., Wodicka, N., McNicoll, V., Saumur, B.M., St-Onge, M.R., and Young, M.D., 2019. U-Pb zircon geochronology of Archean greenstone belts (Mary River Group) and surrounding Archean to Paleoproterozoic rocks, northern Baffin Island, Nunavut; Geological Survey of Canada, Open File 8585, 1 .zip file. <https://doi.org/10.4095/314938>

Publications in this series have not been edited; they are released as submitted by the author

Abstract

Prior to 1:100,000-scale geological mapping conducted in 2017–2018, northern Baffin Island remained a major knowledge gap in the understanding of the northern Rae craton and the tectonic assembly of northeastern Laurentia. Geochronological data in the region was sparse; only four published U-Pb dates existed in the mapping area (~67,000 km²). Resolving the geology and age of the Archean Mary River Group – host to the Mary River iron mine – and the surrounding felsic-to-intermediate gneiss has key implications for the regional tectonic history and mineral prospectivity. In this study, we present new U-Pb zircon ages for 16 samples, including: 3 metavolcanic rocks and a quartzite from the Mary River Group; 2 psammite samples from newly discovered strata near Pond Inlet; 8 felsic-to-intermediate metaplutonic rocks; and 2 mafic metaplutonic rocks. Gneissic granodiorite to quartz diorite that forms the basement to the Mary River Group is dated herein at ca. 2901–2892 Ma. Taking into account previously published data, the age of gneissic basement beneath the Mary River Group is considered to be ca. 2901–2775 Ma. New ages of felsic–intermediate metavolcanic rocks from the Mary River Group define two phases of volcanism at ca. 2830 Ma and ca. 2760–2718 Ma, whereas quartzite from the Mary River Group has a maximum depositional age of ca. 2705 Ma. Psammite from the Pond Inlet area has a similar maximum depositional age of ca. 2720 Ma. Monzogranite and granodiorite and, less commonly, tonalite define an extensive ca. 2731–2706 Ma felsic plutonic suite. Mafic metaplutonic rocks near Pond Inlet, including a layered mafic-ultramafic intrusion, yielded ages of ca. <2720 and >2655 Ma. Late, post-kinematic syenogranite was emplaced at ca. 1792 Ma. U-Pb dates of metamorphic zircon indicate that portions of northern Baffin Island experienced metamorphism during ca. 2.6–2.5 Ga, ca. 1926–1878, and 1850–1820 Ma. The new U–Pb zircon data reinforces lithological and tectonic correlations between northern Baffin Island and the Rae craton in Arctic Canada and West Greenland. Metamorphic U-Pb zircon data also suggest that northern Baffin Island may record tectonothermal activity associated with the Arrowsmith, Ellesmere–Inglefield, and/or Trans-Hudson orogens.

Introduction

Geological mapping was conducted in northern Baffin Island as part of the Geological Survey of Canada's (GSC) GEM-2 North Baffin project, covering the area from Pond Inlet to Mary River in summer 2017, and from Steensby Inlet to the Barnes Ice Cap in summer 2018 (Figs. 1, 2). Previous bedrock mapping of this area includes 1:250,000 scale mapping conducted in the 1960s by the GSC (Jackson and Davidson, 1975; Jackson and Morgan, 1978; Jackson et al., 1978; Davidson et al., 1979), which mainly involved helicopter transects consisting of site visits with ~8 km spacing (Jackson, 2000). Additionally, targeted mapping of selected supracrustal belts was completed during 2003–2005 as part of the North Baffin Project, a collaborative effort between the Canada-Nunavut Geoscience Office (CNGO) and the GSC (Young et al., 2004, 2007; Johns and Young, 2006). Regional 1:100,000 scale mapping undertaken by the GEM-2 North Baffin project involved helicopter-supported foot traverses and site visits. Three new maps have been compiled from this work (Saumur et al., 2018a, b; Skipton et al., 2018a), with an additional five maps in press. Together with related geoscientific research, the new mapping has significantly improved the geoscience knowledgebase and updated the geological framework for northern Baffin Island (Skipton et al., 2017, 2018; Saumur et al., 2018a, b, c). In particular, the project has shed light on the geology of the Archean Mary River Group (MRG) supracrustal rocks, which host the high-grade, large-tonnage Mary River iron deposit currently being mined by Baffinland Iron Mines Corporation.

This report presents new U-Pb zircon ages determined on 12 samples collected during the 2017 GEM-2 North Baffin mapping campaign, and on 4 samples collected by the CNGO during the 2003 targeted mapping campaign. A summary of previous geochronology on northern Baffin Island is provided in Skipton

et al. (2017). Prior to this study, there were only 4 known published U-Pb zircon dates in the study area, including only 2 ages from the prospective MRG (Fig. 3; Jackson et al., 1990; Bethune and Scammell, 2003a). A targeted study by Bethune and Scammell (2003a) in the Ege Bay area (Fig. 2), below the southern border of the GEM-2 North Baffin project area, produced several U-Pb zircon ages for volcano-sedimentary belts and surrounding metaplutonic rocks. Additional ages presented here were required to constrain the ages of MRG supracrustal belts within the study area and their relationship to similar belts in the Ege Bay area, as well as to those along strike on Melville Peninsula (Fig. 1; i.e. Prince Albert and Roche Bay greenstone belts; Corrigan et al., 2013) and west of Committee Bay (i.e. Committee Bay belt; Sanborn-Barrie et al., 2014). To determine the age and cratonic affinity of the crust underlying northern Baffin Island, new U-Pb dates are required on the plutonic rocks and orthogneiss that dominate the study area and surround the MRG. Determining ages of dominant rock units is important for understanding the tectonic evolution of Canada's Arctic, and has potential implications for regional correlations between mineralized domains.

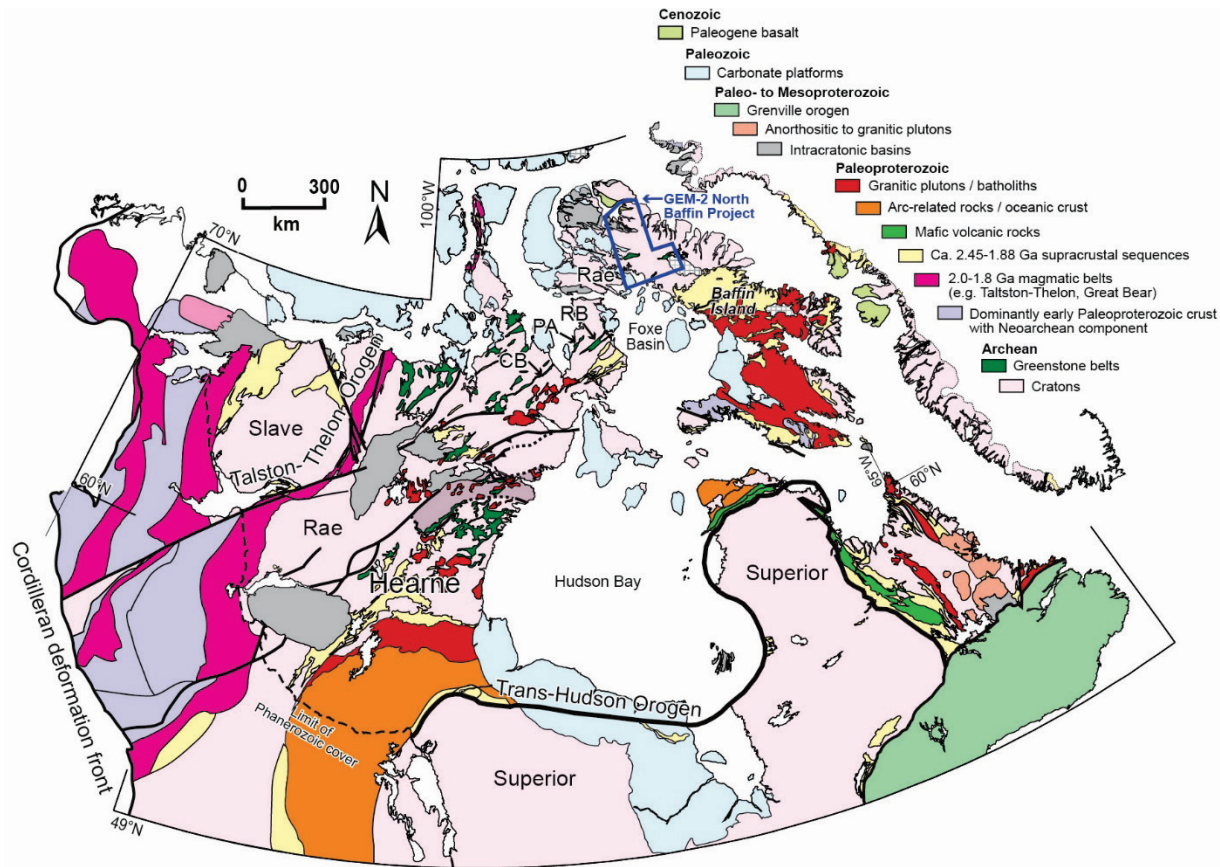


Fig. 1: Regional geological setting of the study area (blue outline) on northern Baffin Island within the context of the eastern Canadian Arctic and western Greenland (modified after Corrigan et al., 2009). Greenland is shown in a pre-drift (pre-late Cretaceous) position as shown by St-Onge et al. (2009 and references therein). RB, Roche Bay belt; PA, Prince Albert Group; CB, Committee Bay belt.

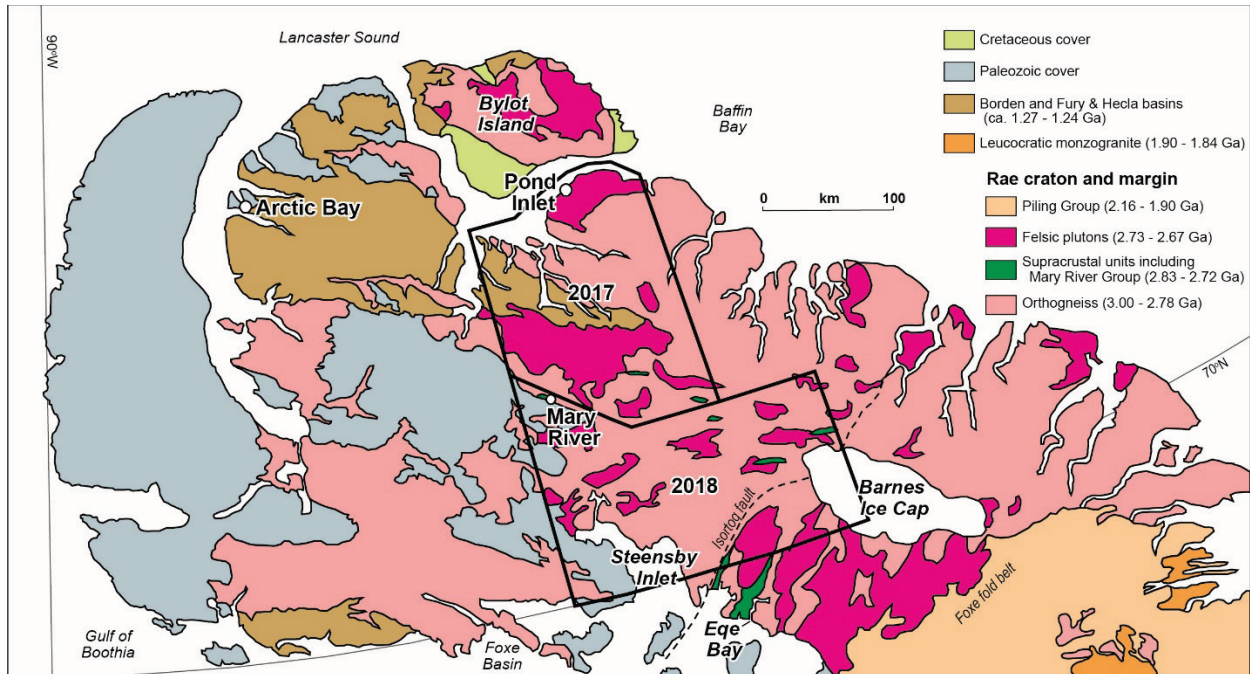


Fig. 2: Generalized geological map of northern Baffin Island, showing the location of 1:100,000-scale bedrock mapping conducted as part of the GEM-2 North Baffin Project during 2017 and 2018 (black outline; NTS sheets 37G, 37F and parts of 38B and 37E). After St-Onge et al., in press.

Geological setting

Archean units of the Pond Inlet – Mary River area are considered to belong to the Prince Albert/Repulse Bay block (or north Rae domain) of the Rae craton, proposed to extend from central Nunavut to at least northern Baffin Island (Fig. 1; e.g., Young et al., 2007; Pehrsson et al., 2011, 2013; Corrigan et al., 2013; Snyder et al., 2013; cf. Jackson and Berman, 2000). In its type area on Melville Peninsula, the correlative Prince Albert/Repulse Bay block is characterized by ca. 2.97–2.60 Ga granite-greenstone belts and Eo- to Mesoarchean cratonic basement (e.g., Wodicka et al., 2011; Corrigan et al., 2013; LaFlamme et al., 2014). To the southeast, Archean crust on northern Baffin Island is bounded by the Isortoq fault (Jackson, 2000) and the Paleoproterozoic Foxe fold belt (Fig. 2), the latter of which represents the northern margin of the ca. 1920–1800 Ma Himalayan-scale accretionary/collisional Trans-Hudson orogen (St-Onge et al., 2006; Corrigan et al., 2009). It has been proposed that the Isortoq fault records northwest-directed thrusting of the Foxe fold belt and underlying basement over Archean crust of northern Baffin Island ca. 1850–1820 Ma (Jackson, 2000; Jackson and Berman, 2000; Bethune and Scammell, 2003b).

The main rock units in the study area are described in detail in Skipton et al. (2017) and Saumur et al. (2018c), and their distribution and geological relationships are presented in recently published maps of the 2017 field area (Fig. 3; Saumur et al., 2018a, b; Skipton et al., 2018a). A brief summary is provided below.

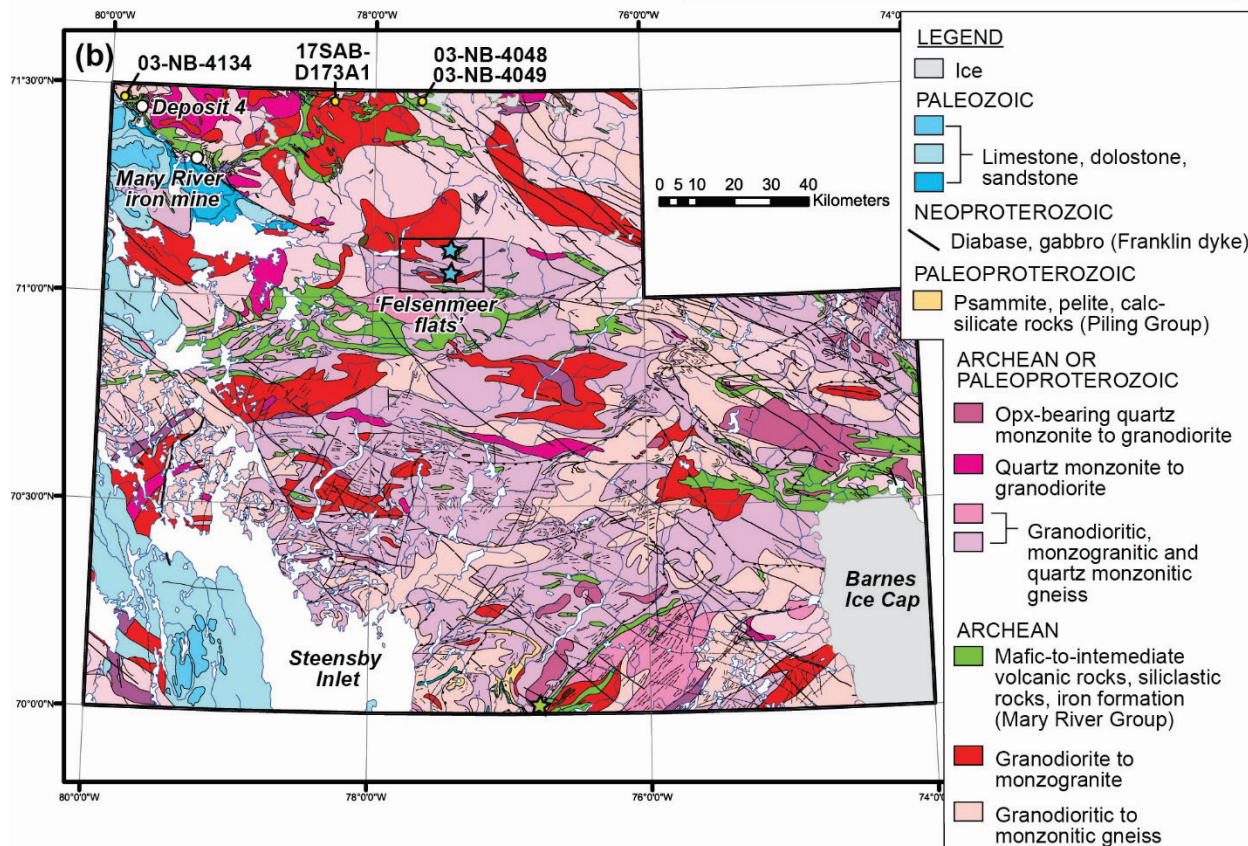
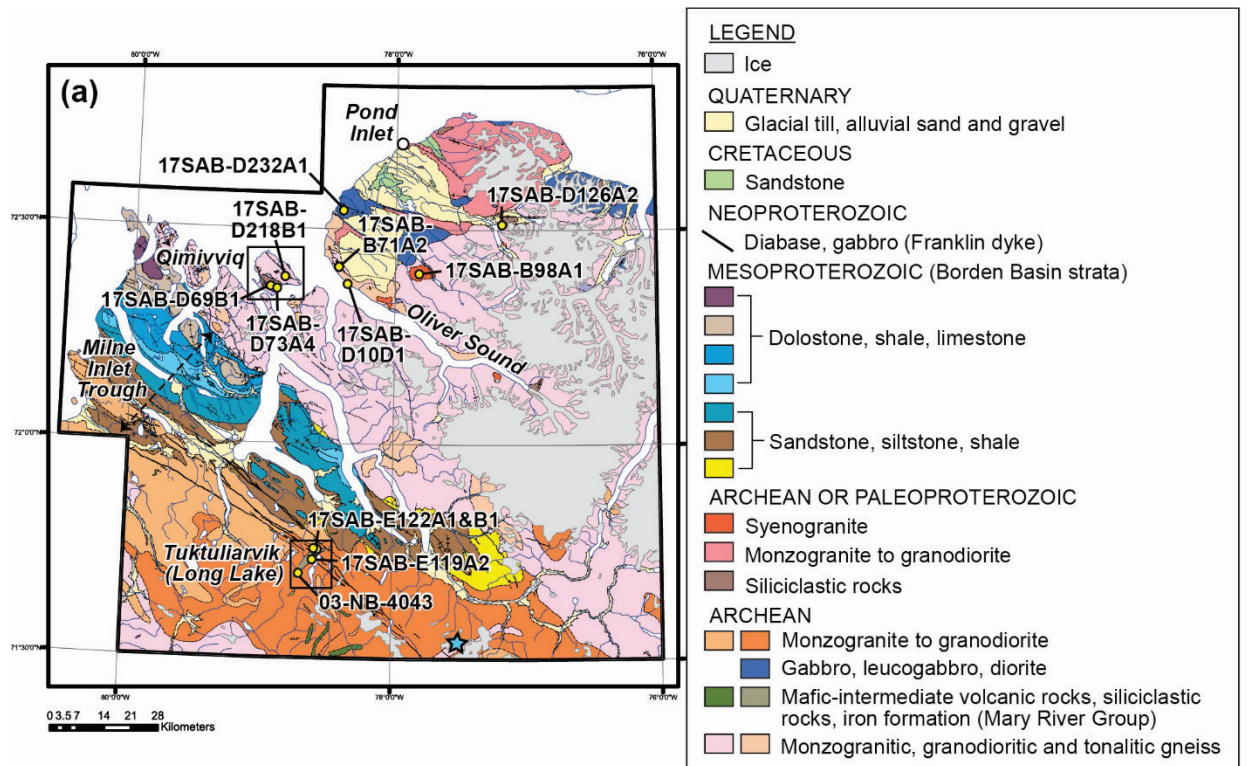


Fig. 3 (previous page): (a) Simplified compilation of the three new 1:100,000-scale bedrock geology maps stemming from the GEM-2 North Baffin 2017 fieldwork in the Pond Inlet area (after Saumur et al., 2018a, b; Skipton et al., 2018a); (b) Generalized geology of the Steensby Inlet – Barnes Ice Cap area, from the compilation map of de Kemp and Scott (1998), based on 1:250,000-scale geological mapping conducted in the 1960s (Jackson and Davidson, 1975; Jackson and Morgan, 1978; Jackson et al., 1978; Davidson et al., 1979). This area was mapped at 1:100,000-scale in 2018 during the second phase of the GEM-2 North Baffin activity. As these new maps have not yet been published, the historical maps are used for illustrative purposes here. Yellow circles indicate locations (with sample numbers) of the U-Pb zircon geochronology samples presented in this Open File. Blue and green stars indicate U-Pb zircon geochronology samples from Jackson et al. (1990) and Bethune and Scammell (2003a), respectively.

Northern Baffin Island is dominantly composed of gneissic Archean felsic plutonic rocks. These include gneissic monzogranite, granodiorite, and tonalite that contain minor mafic-to-intermediate layers and enclaves. A U-Pb zircon crystallization age of $2851 \pm 20/-17$ Ma (thermal ionization mass spectrometry (TIMS)) was previously obtained for tonalite gneiss in the Felsenmeer flats area (Fig. 3b; Jackson et al., 1990), and $\geq 2843 \pm 2$ to 2775 ± 2 Ma protolith ages (TIMS on zircon) for gneiss at Ege Bay (Fig. 2; Bethune and Scammell, 2003a).

The MRG comprises mafic volcanic rocks, siliciclastic units, banded iron formation, felsic to intermediate volcanic rocks, and ultramafic sills/volcanic rocks. Jackson et al. (1990) determined a TIMS crystallization age of $2718 \pm 5/-3$ Ma for dacite in the Felsenmeer flats area (Fig. 3b). In the nearby Ege Bay area, intermediate–felsic MRG volcanism occurred between 2759 ± 2 and 2725 ± 1 Ma (TIMS on zircon; Bethune and Scammell, 2003a). Additionally, zircon from chlorite-garnet schist (likely a meta-volcanic rock) interlayered with iron ore at the Mary River mine (Fig. 3b) yielded a preliminary age of 2748 ± 11 Ma, based on seven analyses by in situ laser ablation-inductively coupled mass spectrometry (Fulcher, 2015).

The study area includes extensive plutons of monzogranite, granodiorite, and syenogranite that exhibit intrusive contacts with orthogneiss, and locally with the MRG. An age of $2709 \pm 4/-3$ Ma has been reported for K-feldspar porphyritic monzogranite (TIMS; Jackson et al., 1990), located ~40 km southeast of the Tuktuliarvik area (Fig. 3a) and hosted by orthogneiss. Granite–granodiorite intrusions bordering the study area near Ege Bay yielded similar TIMS crystallization ages (ca. 2726 to 2714 Ma; Bethune and Scammell, 2003a).

In the northern part of the study area, near Pond Inlet, and in the southern part, between Steensby Inlet and Barnes Ice Cap (Fig. 3), monzogranite and granodiorite locally contain garnet and/or orthopyroxene. In the Pond Inlet area, these intrusions may correlate with charnockitic plutons of the Bylot batholith on Bylot Island (Fig. 2). Enderbite from the Bylot batholith yielded a preliminary zircon age of ca. 2540 Ma (D.J. Scott and G.D. Jackson, unpublished U-Pb sensitive high-resolution ion microprobe (SHRIMP) data; Jackson and Berman, 2000) that may represent the timing of igneous crystallization or, alternatively, a later thermal overprint.

The Pond Inlet area is also characterized by mafic-to-intermediate metaplutonic units, ranging in composition from gabbro to quartz diorite. Layered mafic-ultramafic intrusions occur locally, forming elongate ~1-5 km-sized bodies surrounded by felsic gneiss.

Metasedimentary sequences occurring in the northern part of the study area comprise psammite, semi-pelite, and pelite with rare mafic layers. The relationship between these strata and the MRG to the south has not been previously addressed.

Metasedimentary strata that occur further south, between Steensby Inlet and the Barnes Ice Cap, consist mainly of marble, calc-silicate, quartzite, psammite, semi-pelite, and pelite. These sequences have been assigned to the Paleoproterozoic Piling Group in previous studies (e.g., Jackson, 2000).

All units described above have undergone regional metamorphism at grades ranging from lower-amphibolite to granulite facies. Coeval deformation produced foliations and folding from the microscale to map scale. Regional metamorphism and deformation are described in previous studies (Jackson, 2000; Skipton et al., 2017; Saumur et al., 2018c). Structural fabrics are locally cross-cut by late coarse-grained to pegmatitic dykes and plugs of syenogranite, syenite, and monzogranite.

Archean (\pm Paleoproterozoic) units are nonconformably overlain by Mesoproterozoic clastic and carbonate sequences of the Bylot Supergroup (Jackson, 2000; Turner, 2009, 2011). These strata are within the Milne Inlet Trough (Fig. 3a), part of the Borden rift basin (Jackson and Davidson, 1975). Paleozoic strata of the Cambrian Admiralty Group and Ordovician Brodeur Group lie unconformably upon Archean (\pm Paleoproterozoic) felsic plutonic rocks in the southwestern portion of the study area (Fig. 3b). These sequences include clastic and carbonate rocks, as described by Zhang (2018).

This Open File report presents new SHRIMP and TIMS U-Pb zircon data for the main rock units that constitute northern Baffin Island, including felsic to intermediate gneiss, felsic intrusive suites, and the iron-rich MRG. This report also presents U-Pb zircon data for newly defined units and those that have not yet been dated in the area, including mafic intrusions and metasedimentary sequences near Pond Inlet. In addition, zircon rim ages provide new insights into the timing of regional metamorphism.

U-Pb geochronology sample locations and summary table

As summarized in Table 1, the samples dated in this study include 8 felsic-to-intermediate plutonic rocks, 2 mafic plutonic rocks, 3 felsic-to-intermediate volcanic rocks, and 3 siliciclastic rocks. Sample locations are shown in Fig. 3, and coordinates are given in Appendix 1.

Analytical Methods

All samples were processed at the Geochronology facility of the GSC (Ottawa, Ontario) using standard crushing, grinding, Wilfley™ table, magnetic (Frantz™ isodynamic separator), and heavy-liquid separation methods.

SHRIMP U-Pb zircon geochronology

SHRIMP U-Pb geochronological analyses were conducted on 13 out of 16 samples using the SHRIMP II instrument at the J.C. Roddick Ion Microprobe facility at the GSC (Ottawa, Ontario), following the analytical procedures of Stern (1997) and Stern and Amelin (2003). In general, zircon grains were hand picked (~120 grains per sample) to allow selection of the highest-quality crystals and to capture representative morphological varieties. For detrital samples, zircon grains were selected randomly as best as possible to minimize the effects of sample preparation bias on the detrital zircon age distribution. The

Sample number	Lab number	Method	Lithology	U-Pb zircon ages (Ma)				
				Crystallization	Max. deposition	Min. deposition	Inheritance	Metamorphism
<i>Felsic and intermediate metaplutonic and plutonic rocks</i>								
03-NB-4134	8499	TIMS	Kfs-Pl-phyruc granodiorite	2901 ± 3			ca. 2921	
17SAB-D10D1	12275	SHRIMP	Bt quartz diorite gneiss	2892 ± 4				2709 ± 13
17SAB-D173A1	12277	SHRIMP	Bt monzogranite	2731 ± 3			2814 ± 9	
03-NB-4049	8498	TIMS	Pl-phyruc granodiorite sill	2726 ± 2				
17SAB-E122B1	12160	SHRIMP	Hbl-Bt-Ms monzogranite	2716 ± 4			ca. 3555 to 3400	1878 ± 6
17SAB-D218B1	12159	SHRIMP	Bt tonalite gneiss	2706 ± 3				
17SAB-D69B1	12165	SHRIMP	Grt-Bt±Sil leucogranite sill	ca. 2526-2491				
17SAB-B98A1	12274	SHRIMP	Bt syenogranite	1792 ± 3			2714 ± 6	
<i>Mafic metaplutonic rocks</i>								
17SAB-D232A1	12161	SHRIMP	Grt-Hbl-Cpx gabbro	ca. <2720>2655				1912 ± 5
17SAB-B71A2	12164	SHRIMP	Cpx leucogabbro	2669 ± 11				1926 ± 21 to 1892 ± 9
<i>Metavolcanic rocks (Mary River Group)</i>								
17SAB-E119A2	12162	SHRIMP	Ms rhyolite	2833 ± 3				
03-NB-4043	8496	SHRIMP	Dacite	2829 ± 5				
03-NB-4048	8497	TIMS	Qtz-phyruc dacite	2731 ± 6				
<i>Metasedimentary rocks</i>								
17SAB-D126A2	12276	SHRIMP	Bt psammite		ca. 2720	2592 ± 11		2592 ± 11
17SAB-D73A4	12158	SHRIMP	Bt-Grt-Crd psammite		ca. 3015-2698	ca. <2560>2509		ca. <2560>2509, 1885
17SAB-E122A1	12278	SHRIMP	Ms-Chl quartzite		ca. 2705			

Table 1: Summary of samples analyzed and U-Pb zircon ages determined in this study. See Appendix 1 for the U-Pb zircon data, sample coordinates, and details of analytical conditions.

grains were mounted in 2.5 cm diameter epoxy mounts, together with standard reference materials. Zircon z6266 was used as the primary standard ($^{206}\text{Pb}/^{238}\text{U}$ age = 559 Ma; Stern and Amelin, 2003), and zircon z1242 as the secondary standard ($^{207}\text{Pb}/^{206}\text{Pb}$ age = 2679.7 Ma; B. Davis, unpubl. data). Using 9, 6 and 1 μm diamond compound, the mounts were polished to reveal the middle of the zircon grains.

Backscatter electron (BSE) images of internal features were acquired using a Zeiss EVO 50 or a Tescan Scanning Electron Microscope (SEM) at the GSC (Ottawa, Ontario). Twelve samples were analyzed on 3 mounts during 3 different analytical sessions in 2017–2018, and one sample (03-NB-4043) was analyzed on a separate mount in 2005. Each analysis involved a set of 6 scans over 11 isotope masses of Zr, U, Pb, Th, Yb, and Hf (except for sample 03-NB-4043, which involved measurements on ten isotopes of Zr, U, Th, and Pb, but not Yb and Hf). A ^{16}O -primary beam was used with a spot size between ~ 9 and $23 \mu\text{m}$ and a depth of $\sim 1 \mu\text{m}$. The data were processed offline using customized in-house software for sample 03-NB-4043 or SQUID2 (v. 2.50.11.10.15, rev. 15 Oct. 2011) for all other samples. The Pb composition of the surface blank was used to correct for ^{204}Pb , following the methods of Stern (1997). Further details of analytical conditions during each session are provided in Appendix 1.

TIMS U-Pb zircon geochronology

Isotope dilution thermal ionization mass spectrometry analysis was performed at the GSC on 3 samples collected in 2003 by M.D. Young as part of the CNGO-GSC collaborative project in northern Baffin Island. Zircon crystals were selected for analysis on the basis of morphology, colour, and optical clarity. Prior to analysis, all zircon fractions were air abraded following the method of Krogh (1982). Dissolution in concentrated HF, extraction of U and Pb, and mass spectrometry followed the methods described by Parrish et al. (1987). Mass spectrometric data reduction and numerical propagation of analytical

uncertainties follow Roddick (1987). Procedural blank values for this study were 0.1 pg for U and generally on the order of 3 to 12 pg for Pb. Ages were calculated using the decay constants and natural $^{238}\text{U}/^{235}\text{U}$ ratio of Steiger and Jäger (1977).

Following data reduction of both SHRIMP and TIMS analyses, Isoplot v. 4.15 (Ludwig, 2009) was used to create plots of U-Pb data and calculate regression and weighted average ages. All calculated ages presented in this report are quoted at 2σ uncertainty levels. MSWD refers to Mean Square Weighted Deviation, POF, to probability of fit, and LI, to lower intercept. For two of the three detrital zircon samples (17SAB-D126A2, 17SAB-E122A1), AgeDisplay (Sircombe, 2000) was used to create probability density and histogram plots of $^{207}\text{Pb}/^{206}\text{Pb}$ ages and to calculate maxima. Only one $^{207}\text{Pb}/^{206}\text{Pb}$ age per grain was included in AgeDisplay. For grains with multiple analysis spots, if the MSWD of the weighted average of $^{207}\text{Pb}/^{206}\text{Pb}$ ages of all the spots in the grain was ≥ 2 , the analysis with the oldest apparent age was included in AgeDisplay. If the MSWD was < 2 , the $^{207}\text{Pb}/^{206}\text{Pb}$ weighted average age of all the spots in the grain was used in AgeDisplay.

U-Pb geochronology sample descriptions, results, and age interpretation

Felsic and intermediate plutonic rocks

03-NB-4134 (z8499): K-feldspar- to plagioclase+quartz-phyric granodiorite

This sample was collected from granodiorite in contact with folded supracrustal rocks, including iron formation. These supracrustal rocks have been considered part of the MRG in previous studies, and are informally known as “Deposit 4” (Fig. 3b; e.g., Young et al., 2004). The granodiorite is strongly foliated and lineated, is K-feldspar megacrystic to plagioclase- and quartz-phyric, and contains biotite and hornblende. Where sampled, the granodiorite contains mafic enclaves and schlieren, which increase in abundance toward the contact with the supracrustal rocks. The granodiorite was sampled to provide an age on the gneissic basement to the MRG.

This sample yielded clear, prismatic zircon crystals, ranging from elongate to stubby in shape, and from colourless to pale yellow in colour (Fig. 4a). Five single-grain fractions of elongate crystals were analyzed (A1-A5), as well as two multi-grain fractions (A6, A7). Stubby crystals were analyzed in two single-grain fractions (B1, C1) and two multi-grain fractions (B2, C2).

Eleven fractions yielded $^{207}\text{Pb}/^{206}\text{Pb}$ ages ranging from ca. 2921 to 2879 Ma (Appendix 1), including two fractions that were not considered in age calculations owing to strong reverse discordance and large errors (A4, A5). Fraction A1 (a single elongate prism) was anomalously old (ca. 2921 Ma) relative to the other fractions, possibly owing to the presence of a component of inherited Pb. Five of the remaining 8 analyses (red ellipses) define a regression line with an upper intercept age of 2901 ± 3 Ma (MSWD = 0.71; POF = 0.54; LI = ~ 920 Ma), which is considered to represent the crystallization age of the granodiorite (Fig. 4b). Fractions A7, B2, and C1 (dashed ellipses) plot above the discordia and may have experienced earlier Pb loss.

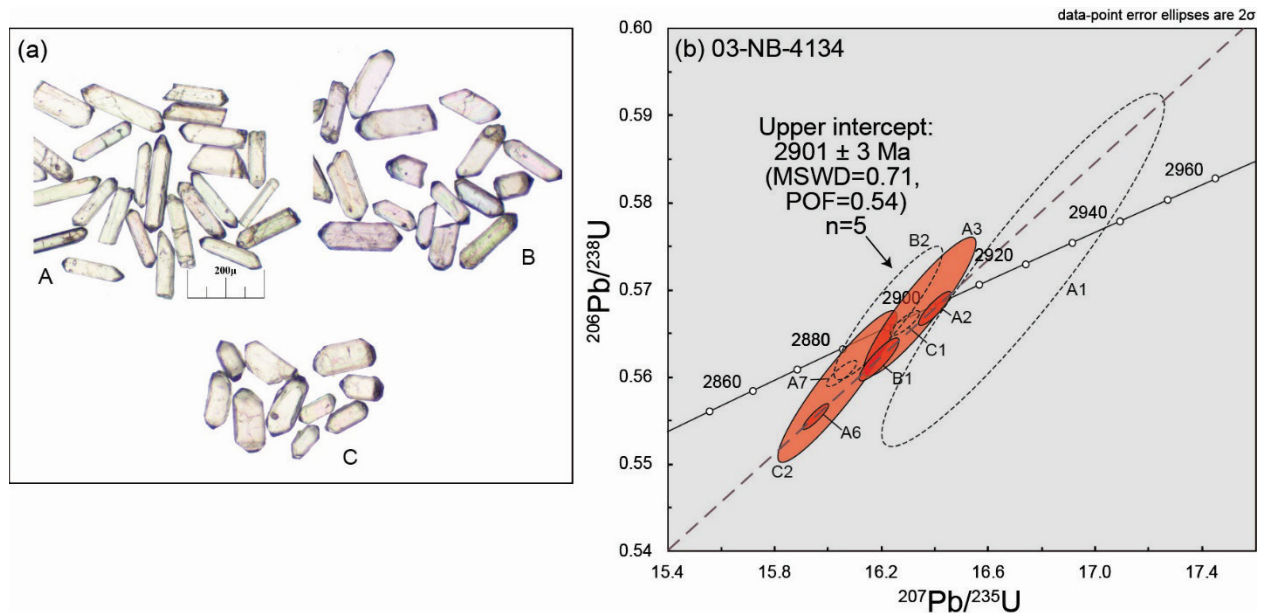


Fig. 4: (a) Transmitted light image of representative zircon grains dated from sample 03-NB-4134. (b) Concordia diagram showing U-Pb zircon data and calculated age from TIMS analyses of the same sample. Fractions A4 and A5 with strong reverse discordance and large uncertainties are not shown. In this and all Concordia plots presented in this report, ellipses with dashed outlines represent analyses that were excluded from age calculations. Coloured ellipses indicate analyses included in calculated ages.

17SAB-D10D1 (z12275): Biotite quartz diorite gneiss

This sample is from a ~1 m-thick band of quartz diorite (Fig. 5a) within gneiss south of Pond Inlet (Fig. 3a), composed of interlayered monzogranite (\pm granodiorite), quartz diorite, and gabbroic enclaves (Fig. 5b). At the sampling site, cross-cutting relationships indicate that quartz diorite is older than granodiorite and monzogranite. The quartz diorite is equigranular, homogeneous, and has a moderate foliation defined by aligned biotite. It was sampled to constrain the age of one of the oldest components of gneissic basement.

Zircon recovered from this sample forms clear to cloudy, stubby to elongate, subhedral to euhedral crystals (Fig. 5c). Many grains are fractured and/or exhibit a light brown colour. In BSE images, most zircon grains display broad, concentric or irregular zoning, and some exhibit dark, homogeneous zones (Fig. 5d, e).

Thirty-five analyses from 23 grains yielded $^{207}\text{Pb}/^{206}\text{Pb}$ ages ranging from ca. 2915 to 2695 Ma (Fig. 5f; Appendix 1). Analyses from mostly zoned material (older grouping of red and dashed ellipses) have U concentrations of 120-441 ppm and yielded the oldest ages, but do not define a single age population. Nine of the twelve oldest analyses from this grouping yielded a $^{207}\text{Pb}/^{206}\text{Pb}$ weighted mean age of 2892 ± 4 Ma (MSWD = 0.78, POF = 0.62; excluding the oldest analysis, which represents an outlier, and the two most precise analyses 12275-113.1 and -121.1). The remaining analyses from this grouping spread along or below the concordia curve, which likely reflects Archean Pb loss at the time of formation of the dark-BSE zircon or more recent Pb loss (or both). Replicate analyses on a number of these grains could not be reproduced, consistent with this interpretation. The 2892 ± 4 Ma age is interpreted as the best estimate

of the crystallization age of the quartz diorite. The five youngest analyses from 4 crystals in the sample (blue ellipses) are from dark-BSE zones, including a dark rim surrounding a light core (grain 13; Fig. 5e), and mostly have lower U concentrations (83-151 ppm) relative to the other analyses. After excluding one of these analyses that is reversely discordant, the four youngest analyses (from 3 crystals) yielded a $^{207}\text{Pb}/^{206}\text{Pb}$ weighted mean age of 2709 ± 13 Ma (MSWD = 1.7, POF = 0.17). This age is considered to represent the timing of a thermal overprint that affected the quartz diorite.

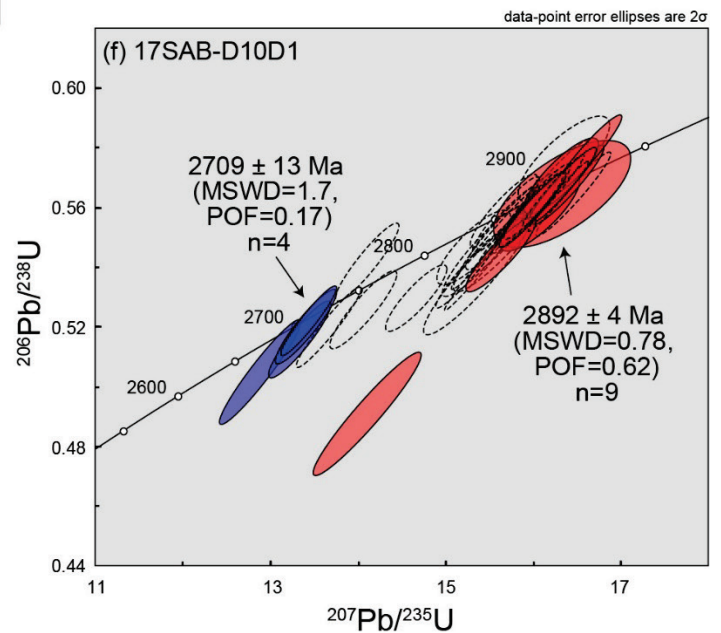
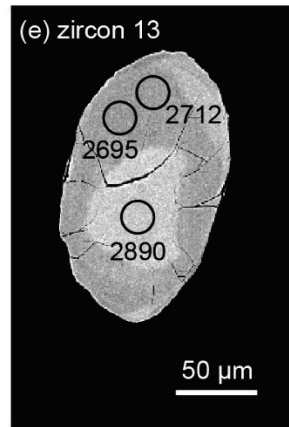
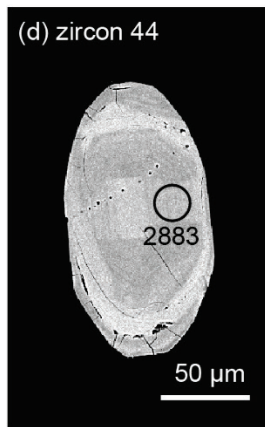
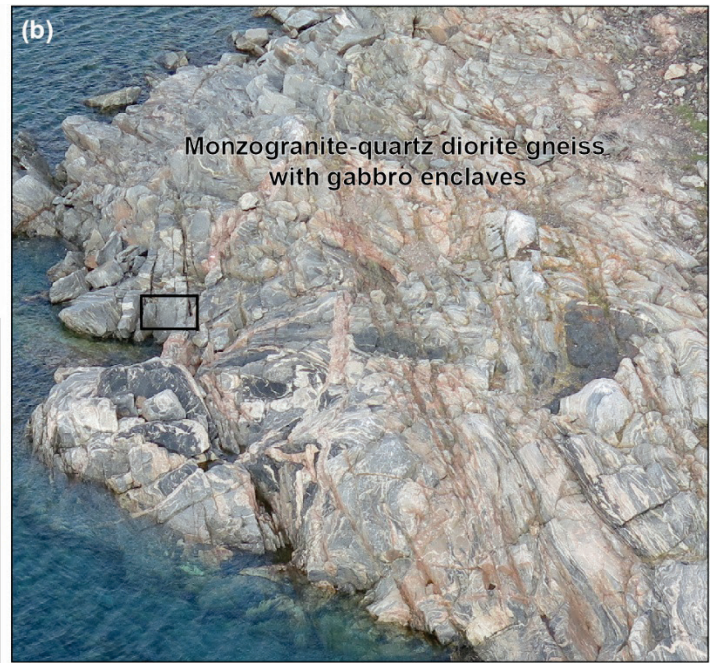


Fig. 5 (previous page): (a) Field photograph of quartz diorite from which sample 17SAB-D10D1 was collected. Felsic veins were avoided during sample collection. Hammer for scale is 35 cm long. (b) Aerial photograph of the gneiss outcrop where the same sample was collected (collection site is outlined in black; field of view of photograph is 30 m). The gneiss is composed of monzogranite (pink), quartz diorite (grey), and gabbro (black). (c-e) Representative images of zircon in sample 17SAB-D10D1, taken in transmitted light (c) and in BSE mode (d, e). In BSE images here and throughout this report, black circles indicate SHRIMP spot locations, which are each labelled with the corresponding $^{207}\text{Pb}/^{206}\text{Pb}$ age (in Ma). (f) Concordia plot showing SHRIMP U-Pb zircon data and calculated ages for sample 17SAB-D10D1. In this and all Concordia plots presented in this report, ages are reported as $^{207}\text{Pb}/^{206}\text{Pb}$ weighted average ages ($\pm 2\sigma$ uncertainty) unless otherwise indicated.

17SAB-D173A1 (z12277): Biotite monzogranite

This monzogranite, collected ~50 km east of the Mary River Deposit 4 (Fig. 3b), is medium grained, equigranular, homogeneous, and contains biotite. It is massive and cross-cuts foliated medium-grained amphibolite along a sharp intrusive contact (Fig. 6a). The amphibolite resembles those that are interlayered with meta-volcanic and metasedimentary units of the MRG elsewhere, although no definitively supracrustal units are exposed in this area. The monzogranite was selected for U-Pb geochronology to provide an age for felsic plutonism in the area east of the Mary River iron deposits.

Zircon recovered from this sample was not abundant, and forms two main morphologies: clear, elongate, commonly fractured, subhedral to euhedral crystals; and clear, stubby to equant grains that are mostly subhedral and rarely well faceted (Fig. 6b). BSE images reveal that for both types of zircon morphologies (Fig. 6c, d), most grains exhibit broad concentric, patchy or sector zoning, and oscillatory zoning is present in some crystals. Several grains have unzoned or broadly zoned cores surrounded by oscillatory-zoned rims (Fig. 6d).

Twenty-seven analyses from 24 zircon grains yielded $^{207}\text{Pb}/^{206}\text{Pb}$ ages ranging from ca. 2817 to 2715 Ma (Fig. 6f; Appendix 1). With the exception of a single stubby, subhedral crystal (grain #82), there is no identifiable difference in age or composition (Th, U, Hf, Yb) between the different zircon morphologies, or between cores and rims. Twenty-three analyses (red ellipses) from 21 crystals produced a $^{207}\text{Pb}/^{206}\text{Pb}$ weighted average age of 2731 ± 3 Ma (MSWD = 2.1, POF = 0.002), which is considered to represent the crystallization age of the monzogranite. Two analyses (green ellipses) from grain #82 (Fig. 6e) produced older $^{207}\text{Pb}/^{206}\text{Pb}$ ages of ca. 2817 and 2810 Ma, with a weighted average age of 2814 ± 9 Ma (MSWD=0.61, POF=0.44). This grain also has a higher Hf content than the rest of the zircon analyzed, and is interpreted to be inherited, potentially from the amphibolite host rock. The remaining 2 analyses (dashed ellipses in Fig. 6f) were not included in age calculations owing to their high discordance (18%; 12277-111.1) or common Pb content in excess of 1% (1.58%; 12277-034.1).

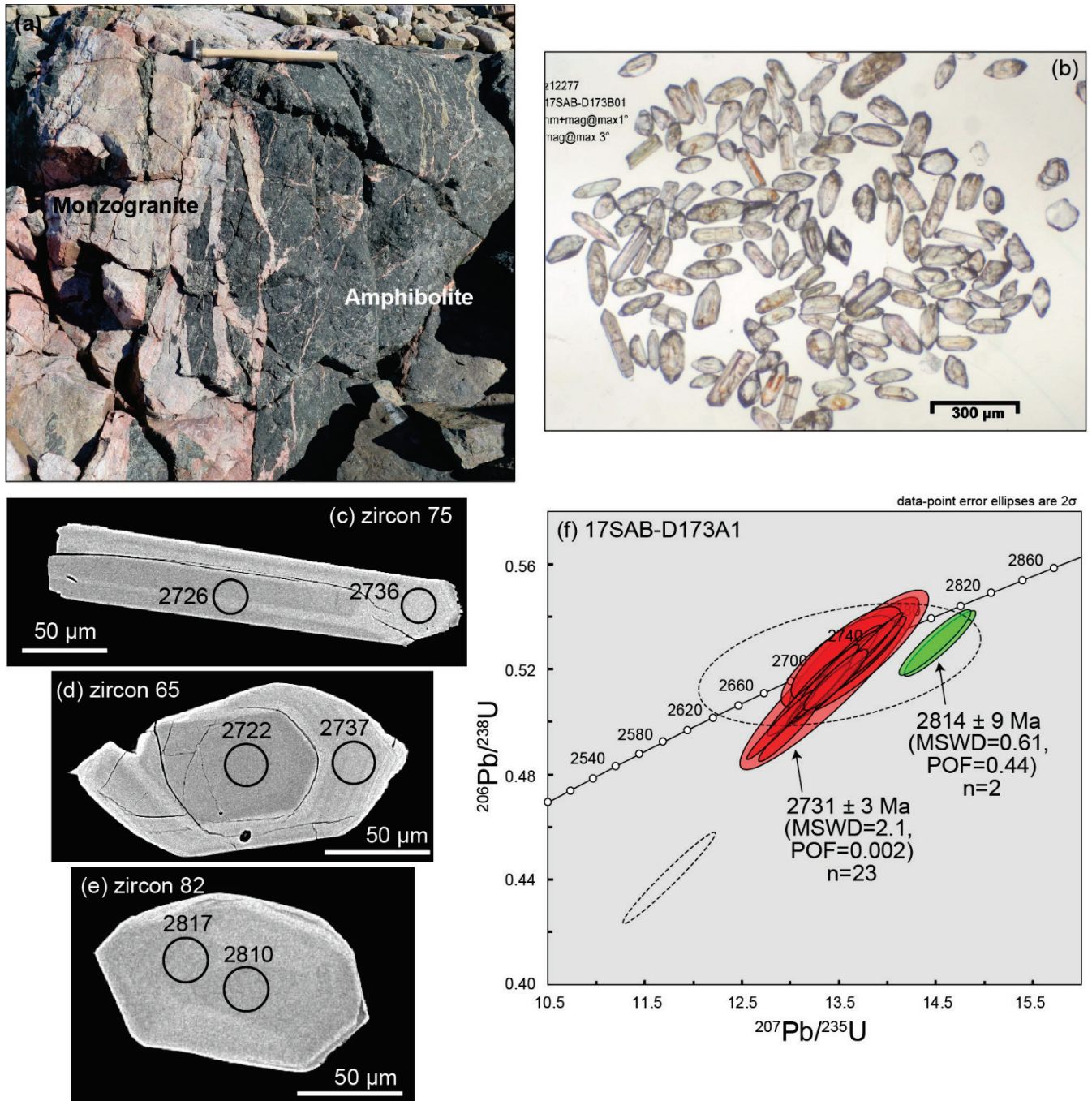


Fig. 6: (a) Field photograph showing the massive monzogranite (from which sample 17SAB-D173A1 was collected) with an intrusive contact into foliated amphibolite. Hammer for scale is 35 cm long. (b-e) Representative images of zircon from the same sample, taken with transmitted light (b) and in BSE mode (c-e). (f) SHRIMP U-Pb zircon data and calculated ages of sample 17SAB-D173A1 presented on a Concordia plot.

03-NB-4049 (z8498): Plagioclase-phyric granodiorite to tonalite sill

Sample 03-NB-4049 was collected ~75 km east of Mary River Deposit 4 (Fig. 3b) from a granodiorite to tonalite sill that exhibits an intrusive contact with mafic-to-intermediate metavolcanic rocks that are considered to be part of the MRG, in which it cross-cuts (at low angles) a foliation that is parallel to volcanic layering (Fig. 7a, b). The granodiorite to tonalite intrusion is strongly lineated, and is composed of plagioclase phenocrysts surrounded by a fine-grained matrix containing muscovite and biotite (Fig. 7c). The field relationships suggest that the granodiorite to tonalite intrusion provides a minimum age for volcanism and foliation development in the MRG at this location and a maximum age for development of the penetrative lineation.

Zircon recovered from sample 03-NB-4049 forms clear and colourless elongate (A1, A2, A3, A5) to stubby prisms (B1, B2), as well as less common pale brown prisms (A4) (Fig. 7d; Appendix 1).

The seven analyzed fractions yielded $^{207}\text{Pb}/^{206}\text{Pb}$ ages between ca. 2723 and 2654 Ma (Fig. 7e; Appendix 1). The three youngest analyses were relatively discordant (1.2-7.4%), attributable to Pb loss. A linear regression through five of the seven analyses (red ellipses) yielded an upper intercept age of 2726 ± 2 Ma (MSWD = 2.3; POF = 0.08; LI = ~1203 Ma), which is considered to be the crystallization age of the plagioclase-porphyritic granodiorite intrusion. Fractions B1 and B2 were excluded from this age calculation because their analyses plot above and below the regression line, respectively.

17SAB-E122B1 (z12160): Biotite hornblende muscovite monzogranite

Monzogranite in the Tuktularvik area (Fig. 3a) contains hornblende, biotite, and muscovite. A weak foliation is defined by aligned mica, and a strong lineation is defined by stretched mineral aggregates. Monzogranite exhibits a sharp contact with quartzite (Fig. 8a; sample 17SAB-E122A1) along the northwestern boundary of the MRG in the Tuktularvik area. The contact is locally irregular, interpreted to have resulted from tectonic interleaving and folding. The monzogranite was sampled to constrain the age of felsic plutonism surrounding the MRG in the Tuktularvik area, and to provide a maximum age for foliation and lineation development.

Many zircon grains recovered from this sample are clear, colourless to light brown, well-faceted, stubby crystals (Fig. 8b). Turbid, fractured grains are also common. In BSE images, zircon crystals are broadly zoned, and some grains exhibit oscillatory zoning within broader zones (Fig. 8c-e). Many grains contain distinct, oscillatory-zoned cores surrounded by unzoned or broadly zoned rims (Fig. 8d).

Thirty-one analyses in 20 zircon grains produced a wide range of $^{207}\text{Pb}/^{206}\text{Pb}$ ages, from ca. 3555 to 1863 Ma (Fig. 8f, g; Appendix 1). Nine (red ellipses) out of 13 analyses from broadly or patchily zoned zircon grains, including from thick rims enclosing cores, yielded a $^{207}\text{Pb}/^{206}\text{Pb}$ weighted average age of 2716 ± 4 Ma (MSWD = 0.86, POF = 0.55; Th/U = 0.01-1.64), interpreted as the crystallization age of the monzogranite. The three youngest analyses excluded from this age calculation are replicate analyses on two zircon grains, which gave non-reproducible results; the spread in ages is likely the result of Pb loss or partial recrystallization (or both). The oldest analysis from this population (12160-077.1), with an age of ca. 2748 Ma, was statistically rejected as an outlier. This analysis is likely a mixed age, as the spot spans part of the zircon core and the thick surrounding rim. Fifteen analyses yielded much older ages, between ca. 3555 and 3154 Ma, and many show discordance that is likely due to Pb loss or mixing of different-aged material (e.g., overlapping core and rim domains in analyses 12160-021.1, -018.1, -054.1). Although some analyses in the older group are from grains with weak, patchy zoning, many are from distinct cores (Fig. 8d), and they are interpreted to represent inherited zircon. Inherited zircon ages are interpreted to range

from ca. 3555 Ma, the age of the oldest, near-concordant analysis, and ca. 3400 Ma, the age of the youngest cluster of near-concordant analyses (green ellipses; Fig. 8f). In addition, 3 analyses from thin outer rims on 3 grains produced ages between ca. 1880 and 1863 Ma, with Th/U ratios of 0.09–0.21. The $^{207}\text{Pb}/^{206}\text{Pb}$ weighted average age of these 3 analyses is 1878 ± 6 Ma (MSWD = 0.86, POF = 0.43), interpreted to reflect the timing of growth of metamorphic zircon rims.

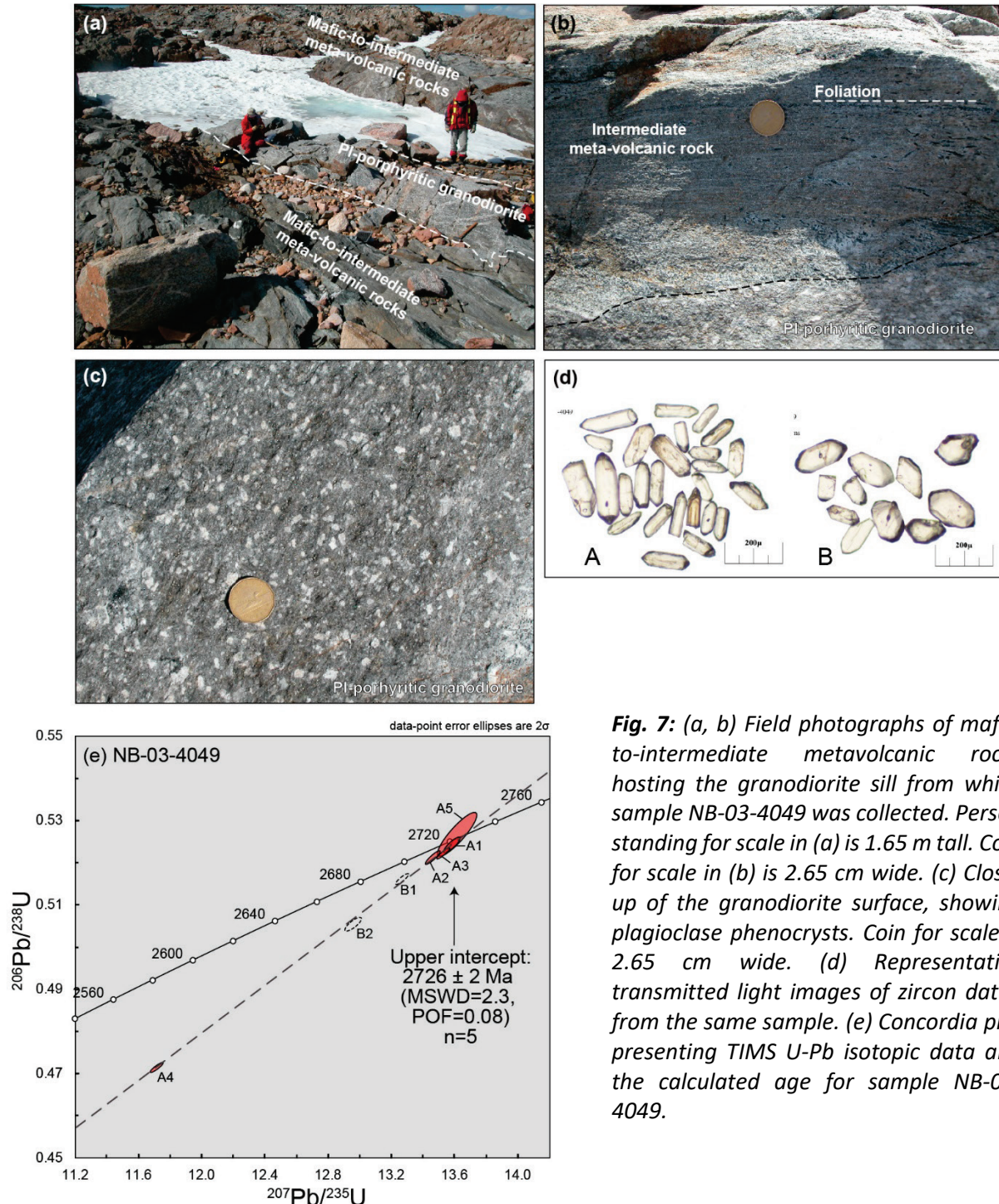


Fig. 7: (a, b) Field photographs of mafic-to-intermediate metavolcanic rocks hosting the granodiorite sill from which sample NB-03-4049 was collected. Person standing for scale in (a) is 1.65 m tall. Coin for scale in (b) is 2.65 cm wide. (c) Close-up of the granodiorite surface, showing plagioclase phenocrysts. Coin for scale is 2.65 cm wide. (d) Representative transmitted light images of zircon dated from the same sample. (e) Concordia plot presenting TIMS U-Pb isotopic data and the calculated age for sample NB-03-4049.

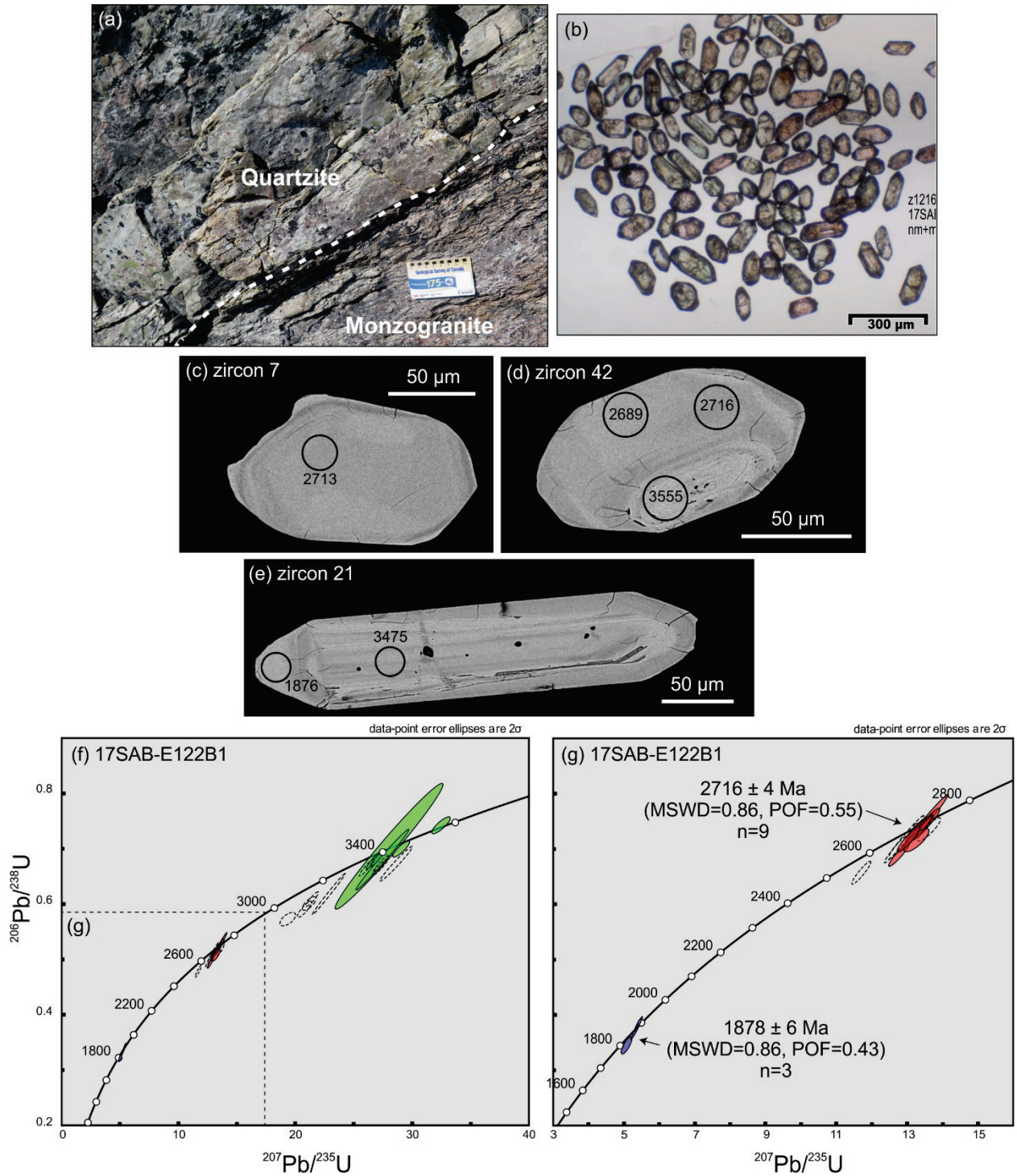


Fig. 8: (a) Field photograph of the contact between the monzogranite from which sample 17SAB-E122B1 was collected, and quartzite from which sample 17SAB-E122A1 was collected. Scale card is 8 cm wide. (b-e) Representative images of zircon from sample 17SAB-E122B1 taken in transmitted light (b) and BSE mode (c-e). (f, g) Concordia plots showing SHRIMP U-Pb zircon data and calculated ages for sample 17SAB-E122B1.

17SAB-D218B1 (z12159): Biotite tonalite gneiss

This tonalite gneiss from the Qimivviq area (Fig. 3a) has a well-developed foliation defined by aligned biotite and compositional banding (Fig. 9a, b). It forms part of a felsic plutonic gneissic complex that overlies metasedimentary rocks along a sharp, northeast-dipping contact (Fig. 9c). Field relationships, including structural fabrics and the protomylonitic nature of the contact, suggest that the contact represents a southwest-vergent thrust fault that juxtaposed tonalite gneiss over metasedimentary rocks (Skipton et al., 2017). The tonalite gneiss was sampled for U-Pb geochronology to provide an age for gneissic basement in the Qimivviq area, and to confirm whether the tonalite gneiss and underlying metasedimentary rocks exhibit an older-over-younger relationship in support of the field interpretation of a thrust fault between the two units.

Zircon recovered from this sample forms mostly clear to slightly turbid, colourless to light brown, elongate to stubby, well-faceted crystals (Fig. 9d). Many grains exhibit oscillatory zoning in BSE images, and some grains have broad or sector zones (Fig. 9e, f).

Twenty-five analyses were acquired from 19 crystals, and yielded $^{207}\text{Pb}/^{206}\text{Pb}$ ages ranging from ca. 2720 to 2563 Ma (Fig. 9g). A $^{207}\text{Pb}/^{206}\text{Pb}$ weighted average age of 2706 ± 3 Ma (MSWD = 1.4, POF = 0.15) was calculated from 16 of the 18 oldest analyses (red ellipses) from the interiors or edges of 16 separate grains (analyses 12159-065.1 and -089.1 were statistically rejected as outliers). This age is considered to be the crystallization age of the tonalite gneiss. The remaining analyses with dashed outlines were not included in age calculations owing to strong discordance.

17SAB-D69B1 (z12165): Biotite-garnet-sillimanite leucogranite

The metasedimentary sequence in the Qimivviq area (Fig. 3a) contains bedding- and foliation-parallel leucogranite layers that range in thickness from centimetre scale to several metres (Fig. 9c). The sample dated here is from a 10 m-thick, folded, coarse-grained, white-weathered leucogranite (Fig. 10a) that contains garnet, biotite, and local sillimanite. The leucogranite encloses brown-weathered patches that are rich in biotite, garnet, and sillimanite, which are interpreted as selvages/rafts of metasedimentary rocks. Considering this field relationship, together with its mineral assemblage, the leucogranite is interpreted as a partial melt of metasedimentary strata (Skipton et al., 2017). The leucogranite was sampled for U-Pb dating to determine the timing of partial melting (i.e., metamorphism) in the metasedimentary rocks at Qimivviq. An age for the leucogranite would also provide a maximum age of folding and a minimum depositional age for the metasedimentary host rocks. The sample was collected several metres away from the metasedimentary host rocks and selvages/rafts.

Zircon in this leucogranite is generally murky brown and forms poorly faceted crystals with 2-4:1 aspect ratios (Fig. 10b). BSE images reveal that most grains have irregular (bumpy) surfaces, are strongly pitted and/or fractured, and exhibit irregular patchy zoning that suggests metamictization (Fig. 10c, d). Some grains display relict concentric or oscillatory zoning in dark BSE domains, although this is typically truncated by patchy, light-BSE domains that may represent recrystallization.

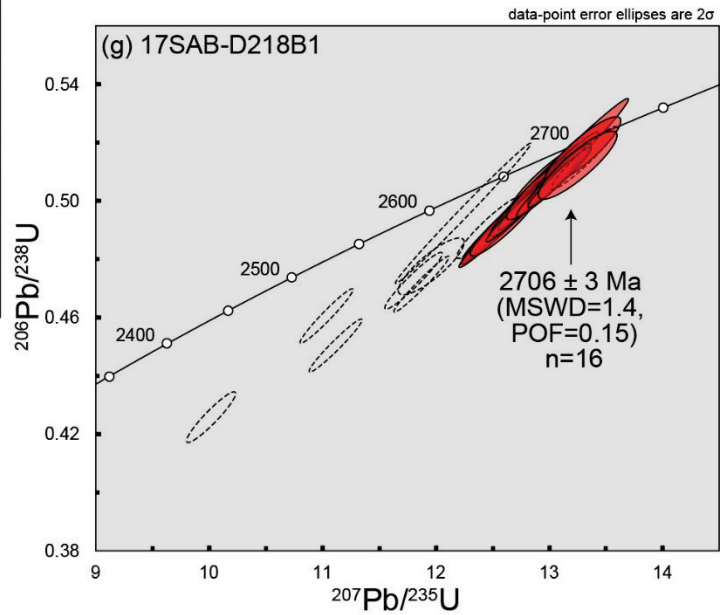
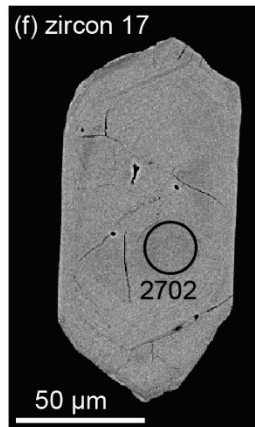
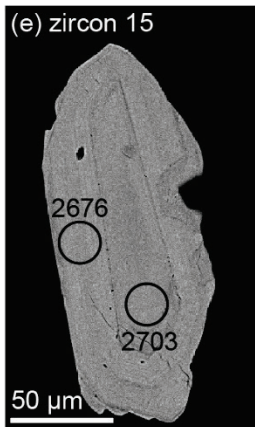
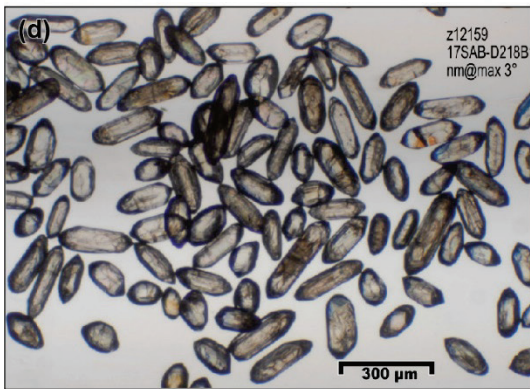


Fig. 9 (previous page): (a) Field photograph of tonalitic gneiss outcrop. Person for scale is 1.65 m tall. (b) Photograph of tonalitic gneiss geochronology sample (17SAB-D218B1). Hammer for scale is 35 cm long. (c) Photograph of the southern cliff face of Qimivviq (Emmerson Island) showing tonalitic gneiss over pelite and leucogranite, separated by a sharp, tectonized contact that has been interpreted as a southwest-vergent thrust fault based on field data. Field of view is ~2.75 km (after Skipton et al., 2017). (d-f) Representative images of zircon from sample 17SAB-D218B1, taken in transmitted light (d) and in BSE mode (e, f). Note that the rim analysis in (e) was not included in the age calculation. (g) SHRIMP U-Pb zircon data and calculated age of sample 17SAB-D218B1 shown on a Concordia plot.

Fourteen zircon grains in sample 17SAB-D69B1 were analyzed using 21 spots in total, mostly in patchy, light-BSE domains. Several analyses of darker BSE domains and relict oscillatory zoning were aborted owing to extremely high ^{204}Pb contents. The 21 analyses yielded $^{207}\text{Pb}/^{206}\text{Pb}$ ages of ca. 2524-2262 Ma (Fig. 10e; Appendix 1). Similar to nearby psammite (sample 17SAB-D73A4, discussed below), the analyses had high U (1419-3913 ppm) and Hf (18335-30295 ppm), and low Th (7-41 ppm) concentrations (Th/U <0.01-0.02). Despite some elevated U contents (> ~2500 ppm) that may suggest the analyzed material was not structurally comparable to the reference zircon (e.g., White and Ireland, 2012), the calibration is considered reliable because all but two (discussed below) analyses in this sample have UO/U ratios (5.9-6.2) that are comparable to those of the reference material (5.9-6.1). Eighteen analyses from the 14 grains (red ellipses) yielded an upper intercept age of 2491 ± 26 Ma (MSWD = 1.13, POF = 0.32). Three analyses were excluded on the basis of strong discordance (12%, analysis 12165-72.2), and reverse discordance and high UO/U relative to the reference zircon in the case of analyses 12165-6.1 and -19.2. The youngest age of zircon recrystallization is estimated at ca. 1885 Ma, based on the results of nearby sample 17SAB-D73A4 (described below). If anchored at 1885 ± 50 Ma, the same 18 analyses from the leucogranite yielded an upper intercept age of 2526 ± 35 Ma (MSWD = 1.60, POF = 0.065). Therefore, the leucogranite is interpreted to have crystallized sometime between ca. 2526 and 2491 Ma.

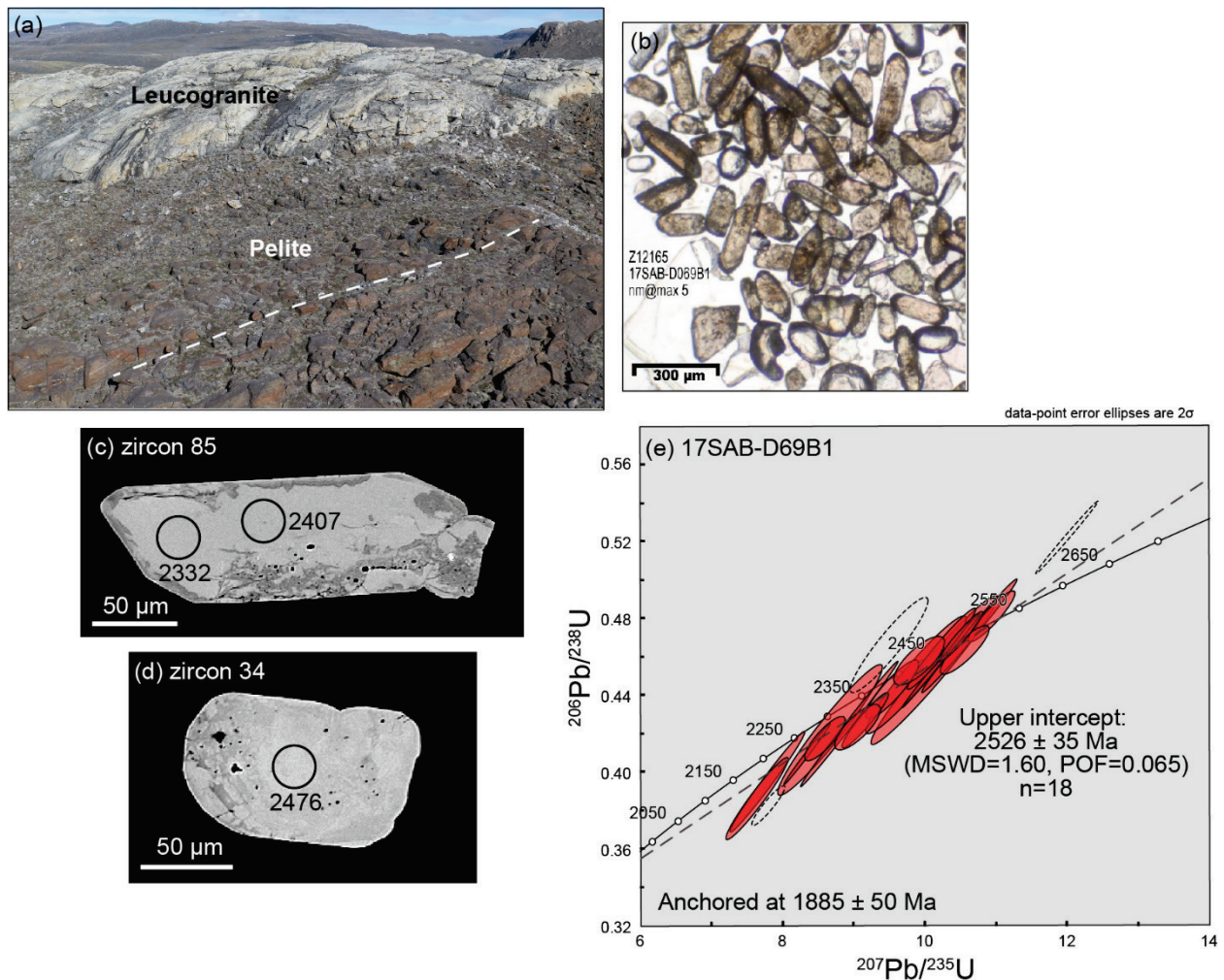


Fig. 10: (a) Field photograph of the leucogranite (white) from which sample 17SAB-D69B1 was collected, in contact with pelite (brown). The white dashed line indicates the orientation of bedding-parallel foliation, which is parallel to the contact between the leucogranite and pelite. Field of view is 7 m. (b-d) Representative images of zircon recovered from sample 17SAB-D69B1, taken in transmitted light (b) and BSE mode (c, d). The clear, colourless, round- to oval-shaped grains in (b) are apatite. (e) Concordia plot presenting SHRIMP U-Pb zircon data and the upper intercept age calculated by anchoring at 1885 ± 50 Ma. Without anchoring, the upper intercept age is 2491 ± 26 Ma. Refer to text for details.

17SAB-B98A1 (z12274): Biotite syenogranite

Sample 17SAB-B98A1 is from a massive, coarse-grained, biotite-bearing syenogranite that forms a 10 km-wide intrusion located approximately 35 km south of Pond Inlet (Fig. 3a). The intrusion exhibits a sharp contact with host tonalitic gneiss, cross-cutting foliation (Fig. 11a), and is the source of numerous off-shooting pegmatitic syenogranite dykes. The syenogranite was selected for U-Pb dating to provide an age for the youngest phase of magmatism that has been identified through field relationships, and to determine the minimum age of regional penetrative foliation in the gneissic host rocks. The sample was collected ~10 m away from the contact with the host tonalitic gneiss.

Zircon grains recovered from this sample are predominantly clear to cloudy, colourless to light brown, euhedral elongate (3-5:1 aspect ratio) and, less commonly, stubby (2:1 aspect ratio) prisms and fragments of these crystals (Fig. 11b, d, e). The sample also contains minor abundances of anhedral grains with irregular or rounded edges, as well as clusters of 2-4 intergrown zircon crystals. Rare subhedral, equant grains were also recovered (Fig. 11c). In BSE, some of the euhedral grains appear unzoned and are uniformly bright (Fig. 11e). However, most grains exhibit a dark-BSE, pitted and/or fractured interior with complex patchy or oscillatory zoning. In several cases, internal zoning appears truncated by a light-BSE domain or rim (Fig. 11d), suggesting that these zones may represent recrystallized domains.

Twenty-two analyses conducted in 21 euhedral, elongate crystals yielded $^{207}\text{Pb}/^{206}\text{Pb}$ ages of ca. 1895-1679 Ma (Fig. 11f, g; Appendix 1). Seven of these analyses (dashed ellipses) are not considered in age calculations owing to strong reverse discordance (up to 67%) or high common Pb contents (>1%) (or both). The latter analyses are from zircon interiors that are dark in BSE and exhibit patchy, irregular or faint oscillatory zoning. The other 15 analyses (red ellipses) are from zircon domains (or unzoned grains) that are light in BSE, and yielded a $^{207}\text{Pb}/^{206}\text{Pb}$ weighted average age of 1792 ± 3 Ma (MSWD=1.2, POF=0.24; Th/U = 0.04-0.13). As this age was determined from domains that appear to have been recrystallized, it is possible that zircon formed prior to ca. 1792 Ma (either from the syenogranite melt, or from country rocks), and underwent recrystallization at ca. 1792 Ma (i.e., the syenogranite may have crystallized before ca. 1792 Ma). However, since the coarse-grained to pegmatitic syenogranite likely represents an evolved melt rich in fluids, it is plausible that zircon underwent fluid-assisted recrystallization late in the syenogranite emplacement history, and that ca. 1792 Ma represents the crystallization age of the syenogranite. This interpretation is preferred here, based on: (1) the predominance of euhedral zircon crystals, which suggest a common igneous source such as the syenogranite; (2) and the absence of older ages from this zircon population, which would be expected if the zircon had crystallized from the syenogranite significantly prior to ca. 1792 Ma, or if the zircon were inherited from country rocks.

There is one exception: duplicate analyses of the core (green ellipses) of a subhedral, equant crystal (grain 13; Fig. 11c) produced an older $^{207}\text{Pb}/^{206}\text{Pb}$ weighted average age of 2714 ± 6 Ma (MSWD=0.047, POF=0.83). Based on its older age, unique morphology, and higher Th/U ratio (0.35) relative to the other zircon in this sample, the ca. 2714 Ma core is interpreted as xenocrystic, possibly inherited from the tonalitic gneiss that hosts the syenogranite.

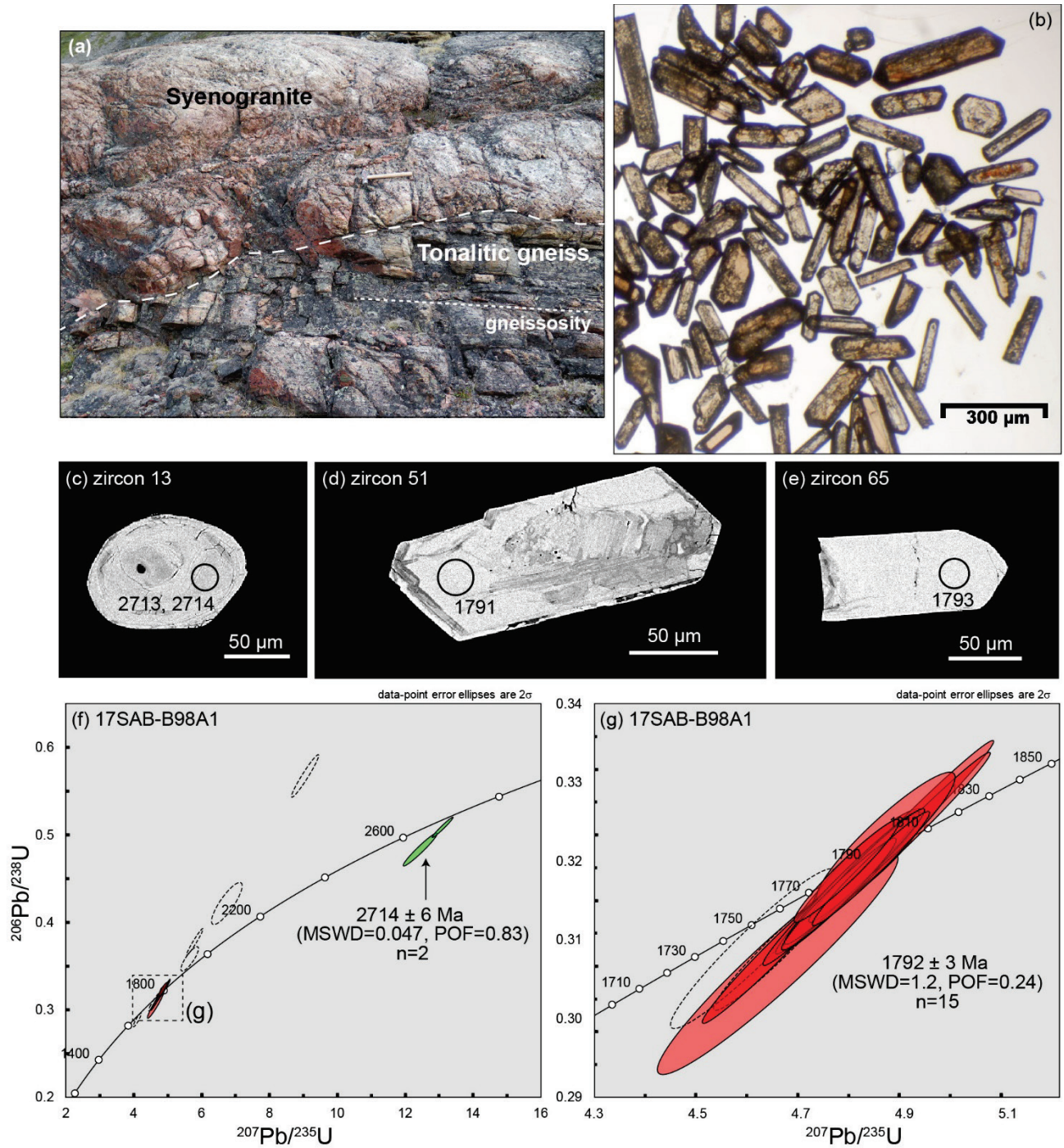


Fig. 11: (a) Field photograph of massive syenogranite (from which sample 17SAB-B98A1 was collected) cross-cutting foliation in tonalitic gneiss. Hammer (35 cm long) is shown for scale at the centre of the photograph. (b-e) Representative transmitted light (b) and BSE (c-e) images of zircon in sample 17SAB-B98A1. (f, g) Concordia plots showing SHRIMP U-Pb zircon data and calculated ages for sample 17SAB-B98A1.

Mafic plutonic rocks

17SAB-D232A1 (z12161): Garnet clinopyroxene gabbro

This sample is from foliated meta-gabbro southwest of Pond Inlet (Fig. 3a) that is composed of hornblende, plagioclase, quartz, clinopyroxene, and garnet. Garnet forms round porphyroblasts that are 2 mm to 3 cm in diameter. The meta-gabbro is characterized by coronae of plagioclase (\pm clinopyroxene) that surround garnet porphyroblasts (Fig. 12a). It was selected for U-Pb geochronology to determine the timing of mafic magmatism in the area surrounding Pond Inlet. A crystallization age for the gabbro would also provide a maximum age for metamorphism and foliation development here.

Zircon from the coronitic gabbro occurs as stubby, poorly faceted, tabular or prismatic to oval-shaped crystals (Fig. 12b). The grains are either clear and colourless, or fractured and light brown to yellow in colour. BSE images reveal that many zircon grains comprise a distinct, light-BSE core, surrounded by a rim that is darker in BSE and is either unzoned or exhibits weak, patchy zoning (Fig. 12c). Numerous other grains are homogeneous or exhibit weak, patchy zoning in BSE and do not contain distinct cores (Fig. 12d). However, some of these grains display a dark-BSE interior surrounded by a subtle light-BSE rim (Fig. 12e).

Forty-eight analyses were completed on 36 zircon crystals. The analyses form three distinct populations, with 30 analyses between ca. 1970 and 1760 Ma, 17 analyses ranging in age from ca. 2677 and 2590 Ma, and a single analysis at 2703 Ma (Fig. 12f; Appendix 1). The oldest analysis (green ellipse) is from a faintly zoned, dark-BSE zircon grain (grain 8) with U, Th, and Yb contents that are distinct from the next oldest group of analyses. Therefore, grain 8 may be a xenocryst. The intermediate group of analyses are from light-BSE zircon cores within mostly prismatic grains, and have lower Hf/Yb ratios relative to grain 8 and the youngest zircon population. Sixteen (red ellipses) out of 17 analyses from this group define a Discordia array with an upper intercept age of 2720 ± 41 Ma (MSWD = 1.4; POF = 0.15; LI = 1483 Ma). The 10 oldest analyses from this group yielded a $^{207}\text{Pb}/^{206}\text{Pb}$ weighted average age of 2655 ± 6 Ma (MSWD = 2.0, POF = 0.032). Given evidence for Pb loss in the prismatic zircon, 2655 ± 6 Ma is interpreted as a minimum estimate for the crystallization of the gabbro and 2720 ± 41 Ma as a maximum estimate. As this age range encapsulates the oldest analysis in the sample (from grain 8, ca. 2703 Ma), grain 8 could possibly represent a chemically distinct zircon belonging to the ca. 2720–2655 Ma population rather than a xenocryst. However, this analysis is statistically rejected from the weighted average age calculation of the 11 oldest analyses, supporting its distinctly older age that is consistent with a xenocrystic origin. It follows from this interpretation that the crystallization age of the gabbro is likely to have been closer to ca. 2655 Ma than ca. 2720 Ma. The analyses in the youngest population are from zircon rims, as well as from colourless, oval-shaped grains that lack cores and are homogeneous or exhibit weak, patchy zoning in BSE. Twenty-eight (blue ellipses) out of 30 of these analyses produced a $^{207}\text{Pb}/^{206}\text{Pb}$ weighted average age of 1912 ± 5 Ma (MSWD = 1.2, POF = 0.20), and have low Th/U and high Hf/Yb ratios compared to zircon cores. Based on the zircon chemistry and morphology, this age is interpreted to represent the timing of growth of zircon rims and whole crystals during metamorphism. The two youngest analyses (ca. 1760, 1847 Ma) are not included in age calculations owing to low UO/U ratios and high common Pb (1.53-1.63%).

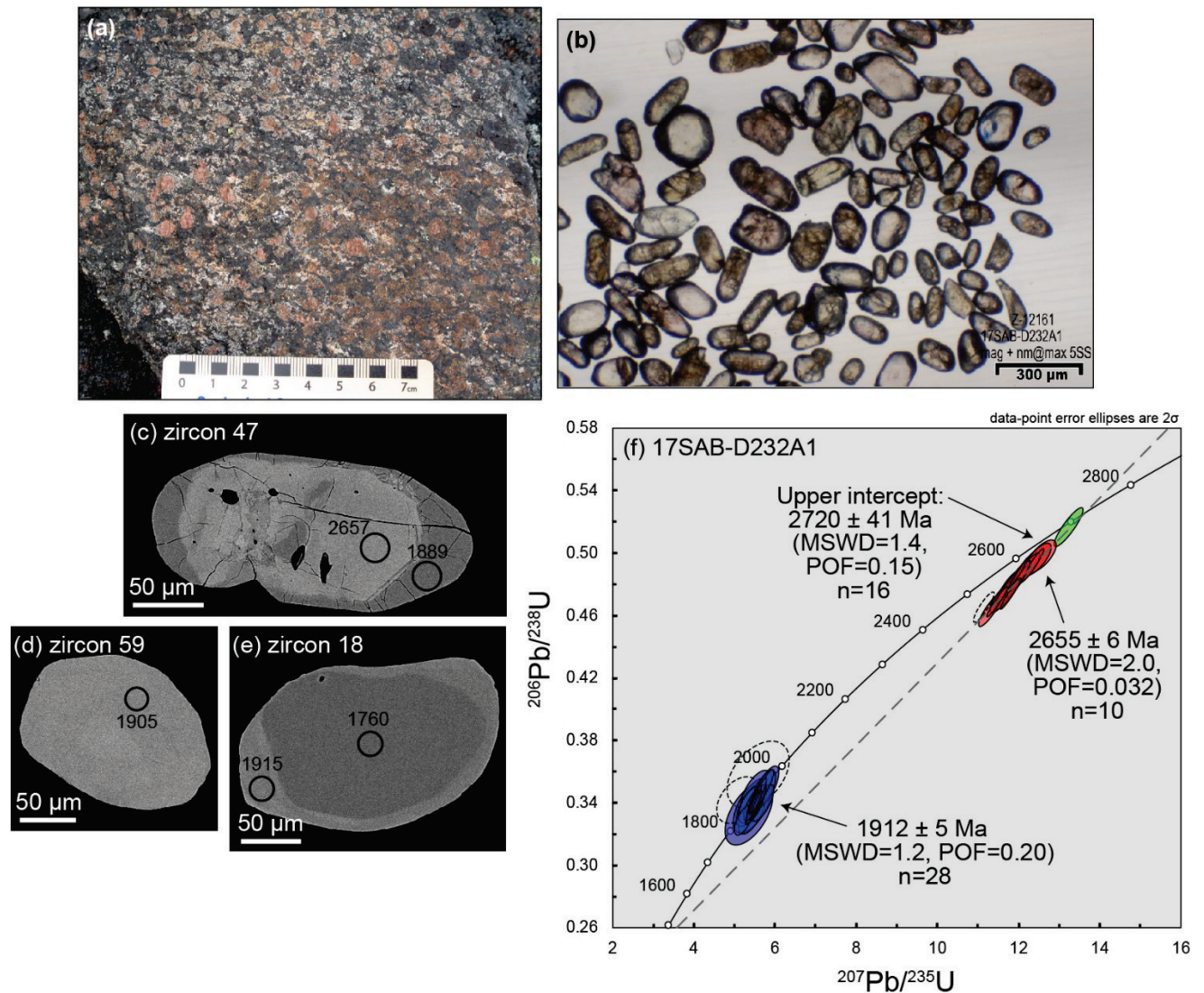


Fig. 12: (a) Field photograph of the gabbro from which sample 17SAB-D232A1 was collected, containing garnet porphyroblasts with plagioclase coronae. (b-e) Representative transmitted light (b) and BSE (c-e) images of zircon recovered from sample 17SAB-D232A1. Note that the ca. 1760 Ma core analysis in (e) was not included in age calculations owing to low UO/U ratio, high common Pb, and being younger than the rim analysis. (f) Concordia plot showing SHRIMP U-Pb zircon data and calculated ages for sample 17SAB-D232A1.

17SAB-B71A2 (z12164): Layered leucogabbro

This leucogabbro is from a 0.5 x 2 km-sized layered mafic-ultramafic intrusion that crops out along Oliver Sound, located approximately 15 km south of the garnet-clinopyroxene gabbro 17SAB-D232A1 (Fig. 3a). The intrusion is composed of alternating 5-100 m-thick layers of gabbro and pyroxenite, with subordinate dm-scale layering characterized by changes in modal abundances of plagioclase and pyroxene.

Disseminated sulphide (pyrite, pyrrhotite) occurs locally. The leucogabbro sample dated here mainly comprises clinopyroxene, plagioclase, and hornblende with minor quartz. It is characterized by alternating plagioclase- and pyroxene-rich layers that are interpreted as primary igneous layers (Fig. 13a). The leucogabbro was sampled to provide a crystallization age for the layered mafic-ultramafic intrusion. As similar intrusions have been shown to host magmatic Ni-Cu-PGE mineralization (e.g., Paleoproterozoic Raglan deposit of northern Québec; Lesher, 2007), the age of the leucogabbro may help to evaluate the potential for economic mineralization on northern Baffin Island.

Most zircon grains in this sample form clear, colourless, equant (round) to oval-shaped crystals that are poorly-faceted (Fig. 13b, c). In lower abundances, zircon forms pale brown, stubby (2:1 aspect ratio) subhedral to anhedral grains and fragments (Fig. 13b-e). The dominant morphology of round to oval-shaped grains are unzoned in BSE, except for subtle, partial, light-BSE rims or more extensive bright domains exhibited by some grains. In contrast, the stubby subhedral to anhedral crystals are strongly fractured and display complex patchy or oscillatory zoning, typically surrounded by an unzoned rim.

Thirty-eight analyses were conducted across 24 grains, and yielded $^{207}\text{Pb}/^{206}\text{Pb}$ ages of ca. 2684 to 1705 Ma (Fig. 13f; Appendix 1). Replicate analyses from the interiors of 3 stubby, subhedral zircon crystals from the Archean group of analyses have high Th/U ratios (0.37-0.58) relative to the Paleoproterozoic analyses in this sample. Eight out of 9 analyses from this morphological group yielded a $^{207}\text{Pb}/^{206}\text{Pb}$ weighted average age of 2665 ± 13 Ma (MSWD=13, POF=0.00). The data exhibit excess scatter in part owing to Pb loss, especially in the three youngest and non-reproducible analyses, and some highly precise analyses. Excluding the three youngest analyses yielded a Tukey's biweight mean of 2669 ± 11 Ma (red ellipses), considered as the best estimate of the crystallization age of the layered gabbro given that this method is more resistant to outliers.

The Paleoproterozoic group of analyses had low Th/U ratios (<0.01-0.06) relative to the Archean analyses. Seven analyses from the Paleoproterozoic group were not considered in age calculations owing to excessive errors, % discordance ($\geq 10\%$) and/or high common Pb, or were statistically rejected from age calculations. Of the nineteen analyses (in 15 crystals) included in age calculations, most were from round to oval-shaped zircon grains with weak or absent zoning, except for seven that were from rims (grains 47, 116) or light-BSE domains (likely recrystallized zones) within stubby subhedral crystals (grains 16, 65, 90, 93, 128). The analyses show highly variable precision owing to highly variable U concentrations (15-2027 ppm), which correlate to the subtle core-rim zoning exhibited by some of the round zircon grains (Fig. 13c) or to the light-BSE recrystallized zones (Fig. 13e). By separating the analyses into two subgroups based on U concentration and textures, the low U analyses (15-96 ppm; blue ellipses) from unzoned dark-BSE cores produced a $^{207}\text{Pb}/^{206}\text{Pb}$ weighted average age of 1926 ± 21 Ma (MSWD=1.2, POF=0.27), whereas the high U analyses (211-2017 ppm; pink ellipses) from light-BSE rims or recrystallized domains yielded a Tukey's biweight mean age of 1892 ± 9 Ma. These ages may indicate that zircon-forming metamorphic reactions in the gabbro began as early as 1926 ± 21 Ma and that metamorphic recrystallization occurred at 1892 ± 9 Ma.

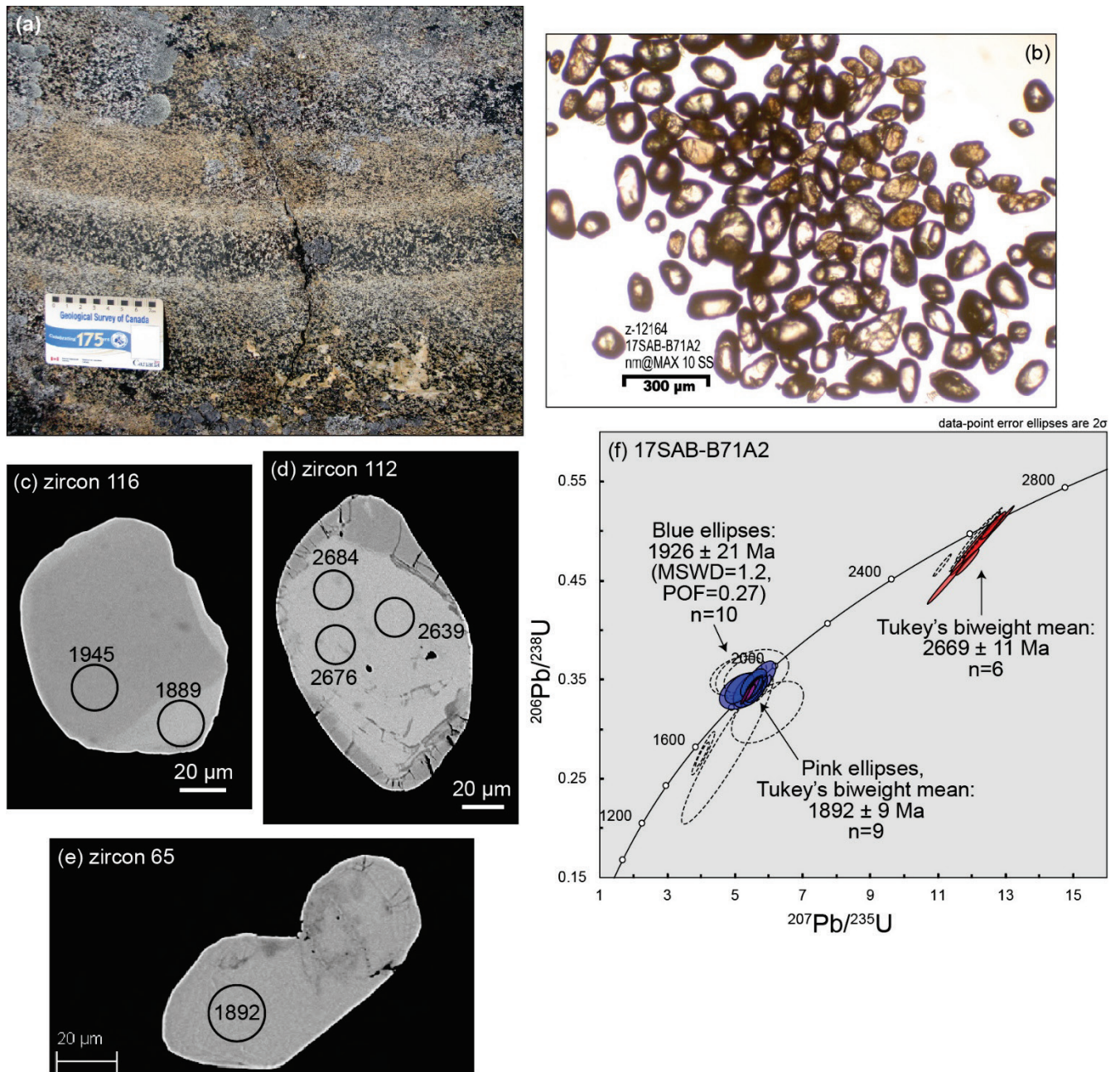


Fig. 13: (a) Field photograph of compositional layering in the mafic-ultramafic intrusion from which sample 17SAB-B71A2 was collected. Scale card is 8 cm wide. (b-e) Representative images of zircon in sample 17SAB-B71A2 taken in transmitted light (b) and BSE mode (c-e). (f) Concordia plot of SHRIMP U-Pb zircon data and calculated ages for sample 17SAB-B71A2.

Metavolcanic rocks of the Mary River Group

17SAB-E119A2 (z12162): Rhyolite

Meta-rhyolite from the Tuktuliarvik area (Fig. 3a) is pale yellow to cream coloured, very fine grained to aphanitic, and strongly foliated and lineated (Fig. 14a). Foliation is defined by aligned muscovite and 1-2 mm-thick bands of quartz, and lineations are defined by aligned muscovite and stretched (rodded) groundmass. The meta-rhyolite is stratigraphically overlain by banded iron formation (Fig. 14b), and was targeted for U-Pb geochronology to provide an age for volcanism and associated iron deposition in the MRG.

Zircon occurs as clear to turbid, colourless to pale brown, subhedral to euhedral, stubby to elongate prismatic crystals (Fig. 14c). Some grains are strongly fractured. In BSE images, most grains exhibit oscillatory zoning, whereas others display faint broad zoning (Fig. 14d, e).

Twenty-five analyses were conducted on 21 crystals, and returned $^{207}\text{Pb}/^{206}\text{Pb}$ ages between ca. 2848 and 2810 Ma (Fig. 14f; Appendix 1). Twenty analyses (red ellipses) from 17 grains, with Th/U ratios ranging from 0.23 to 0.81, yielded a weighted mean $^{207}\text{Pb}/^{206}\text{Pb}$ age of 2833 ± 3 Ma (MSWD = 1.40, POF = 0.10). This is interpreted as the crystallization age. The five other analyses (dashed ellipses) were not included in the age calculation owing to high common Pb contents (>1%), very large errors, and (or) strong discordance.

03-NB-4043 (z8496): Dacite

Meta-dacite from southwest of the Tuktuliarvik area (Fig. 3a) is overlain by amphibolite (Fig. 15a) and underlain by quartzite and meta-quartz arenite. The meta-dacite is homogeneous to lapilli tuffaceous, has a grey-blue fresh surface and a light blue to pale pink weathered surface (Fig. 15b). It was sampled to determine the age of volcanism in the MRG.

Zircon grains recovered from this sample are predominantly clear, colourless, stubby, euhedral to subhedral prismatic crystals (Fig. 15c). The sample also contained smaller, stubby to equant, subhedral to anhedral grains and crystal fragments. Many grains are fractured and some exhibit a murky brown colour. Zircon grains exhibit well-developed oscillatory zoning in BSE images, and some grains also have sector zones (Fig. 15d).

Sixteen zircon crystals were analyzed using seventeen analyses, which produced $^{207}\text{Pb}/^{206}\text{Pb}$ ages ranging from ca. 2846 to 2665 Ma (Fig. 15e; Appendix 1). Thirteen analyses from 13 grains (red ellipses) yielded a $^{207}\text{Pb}/^{206}\text{Pb}$ weighted average age of 2829 ± 5 Ma (MSWD=0.97, POF=0.48), taken as the crystallization age. Four analyses (dashed ellipses) were statistically rejected from the age calculation or excluded owing to strong discordance.

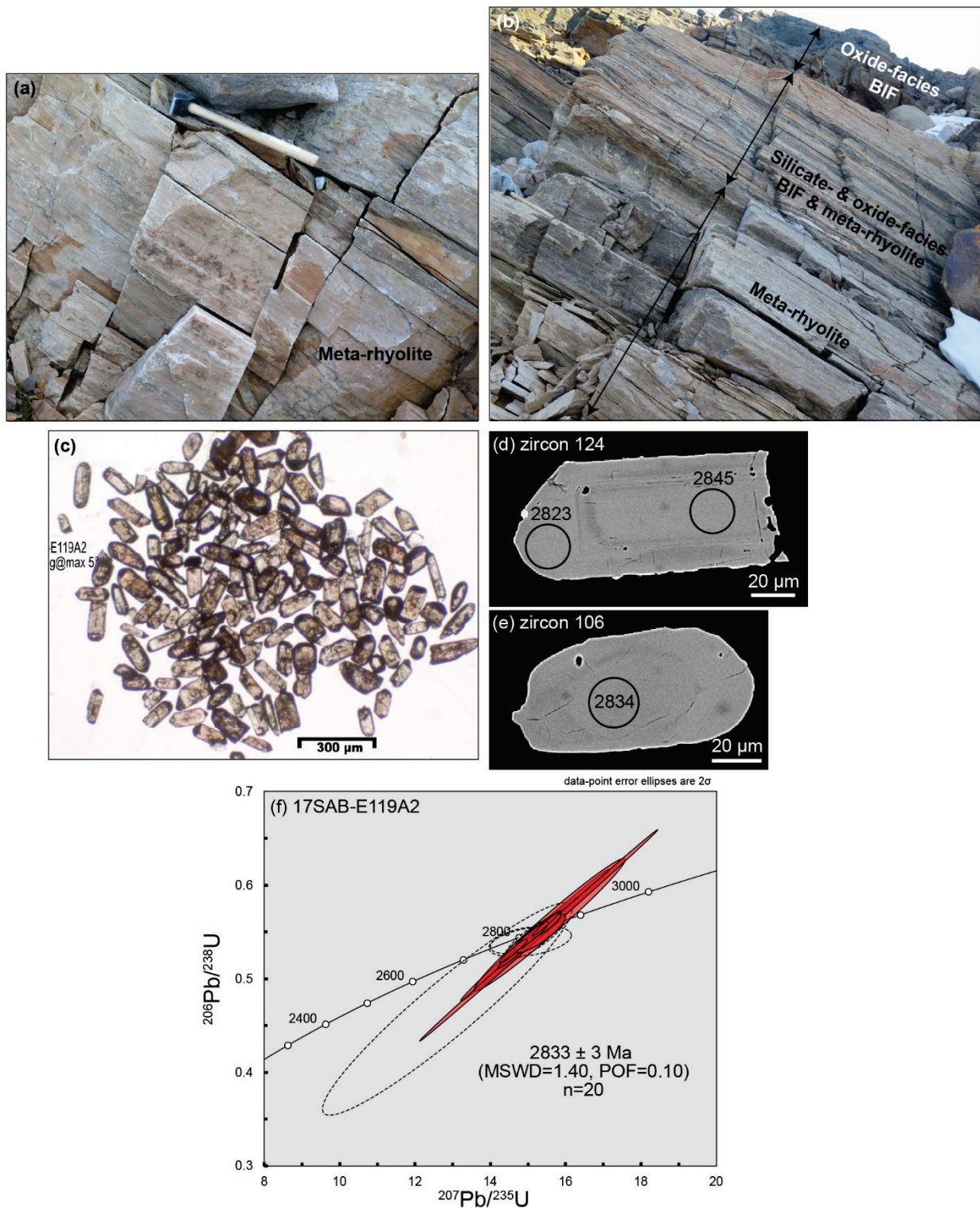


Fig. 14: (a) Field photograph of meta-rhyolite, where sample 17SAB-E119A2 was collected. (b) Field photograph of the same meta-rhyolite, in stratigraphic contact with overlying banded iron formation. Hammer for scale in (a) and (b) is 35 cm long. (c-e) Representative images of zircon recovered from sample 17SAB-E119A2, taken in transmitted light (c) and BSE mode (d, e). (f) Concordia diagram showing SHRIMP U-Pb zircon data and the calculated age of sample 17SAB-E119A2.

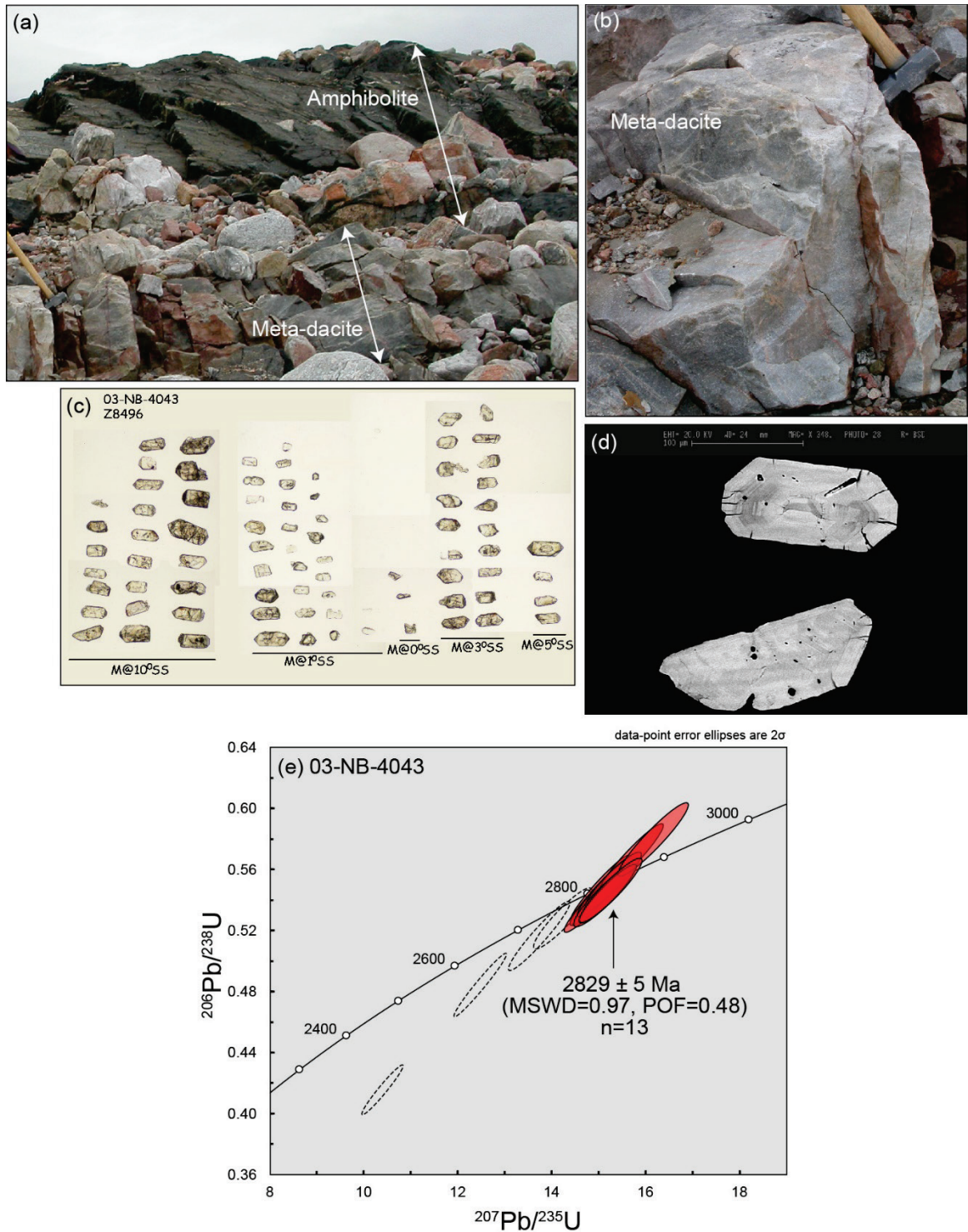


Fig. 15: (a) Field photograph showing meta-dacite from which sample 03-NB-4043 was collected, overlain by amphibolite. (b) Field photograph of collection site of meta-dacite geochronology sample. Hammer for scale in (a) and (b) is 55 cm and 20 cm long, respectively. (c) Transmitted light image of representative zircon crystals from the same sample. (d) Representative BSE images of zircon dated in sample 03-NB-4043. (e) Concordia plot showing SHRIMP U-Pb isotopic data and the calculated age for the same sample.

03-NB-4048 (z8497): Quartz-phyric lapilli dacite

This sample is from homogeneous to lapilli tuffaceous meta-dacite (Fig. 16a) that is interlayered with iron formation (Fig. 16b). The sample was collected approximately 60 km east of the Mary River iron mine (Fig. 3b) and approximately 500 m northwest of sample 03-NB-4049. The meta-dacite has a blue-grey fresh surface and contains rare 1-3 mm ovoid quartz crystals. The dacite was targeted for U-Pb dating to obtain the age of volcanism and iron deposition in the MRG.

Zircon crystals recovered from the meta-dacite include clear, colourless to pale brown prisms (A1, A2), stubby prisms (B1, B2), as well as distinctly large prisms (C1) and their tips (C2) (Fig. 16c).

Five of the six analyzed fractions yielded $^{207}\text{Pb}/^{206}\text{Pb}$ ages ranging from ca. 2730 and 2706 Ma, whereas the strongly discordant fraction (A2) yielded a younger age of ca. 2647 Ma (Fig. 16d; Appendix 1). A $^{207}\text{Pb}/^{206}\text{Pb}$ weighted average age of 2728 ± 6 Ma (MSWD = 1.6, POF = 0.20) was produced from the three oldest fractions, comprising a multi-grain fraction of 8 clear stubby prisms (B1), a large clear prism (C1) and the tip of a large pale brown prism (C2). A linear regression through all the data yielded an upper intercept of 2731 ± 6 Ma (MSWD = 1.4; POF = 0.24) and a lower intercept of 1802 ± 96 Ma. The upper intercept age is considered to be the volcanic crystallization age of the meta-dacite. This interpretation is supported by the fact that 2731 ± 6 Ma is within 2σ uncertainties of the weighted mean age 2728 ± 6 Ma and the oldest, most concordant and precise analysis (C1; 2730 ± 3 Ma).

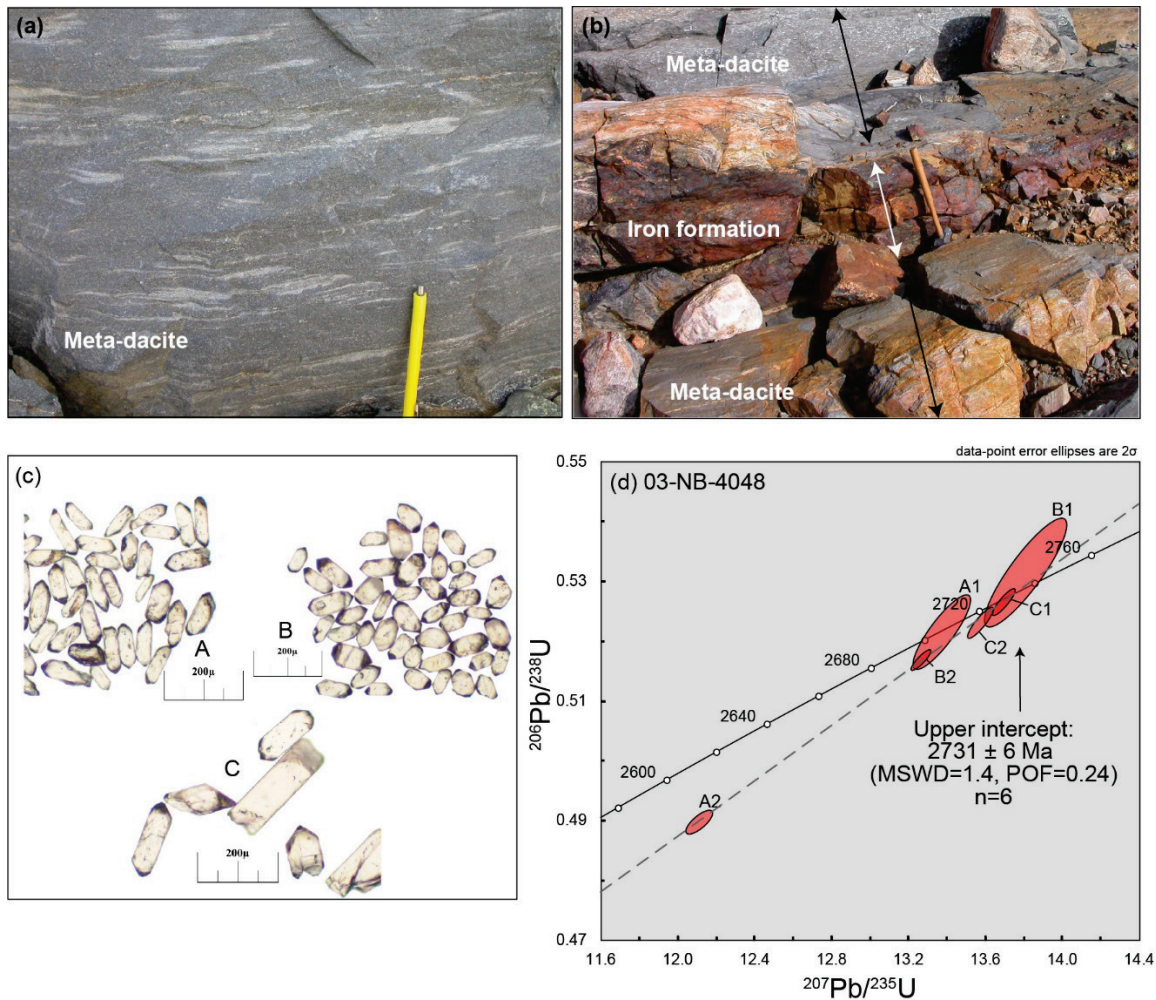


Fig. 16 (previous page): (a, b) Field photographs of the meta-dacite from which sample 03-NB-4048 was collected, interlayered with iron formation. Magnetic pen (a) and hammer (b) for scale are 12 and 35 cm long, respectively. (c) Representative transmitted light images of zircon grains dated from the same sample. (d) TIMS U-Pb zircon isotopic data and calculated age for sample 03-NB-4048 presented on a Concordia diagram.

Metasedimentary rocks

17SAB-D126A2 (z12276): Biotite psammite

Psammite from southeast of Pond Inlet (Fig. 3a) is equigranular and homogeneous, and is composed of quartz, plagioclase, and biotite. Psammite forms 10-30 cm layers alternating with layers of biotite semipelite and bands of coarse-grained biotite-garnet leucogranite (Fig. 17a-c). Foliation in the psammite is defined by aligned biotite. The metasedimentary sequence is cross-cut by a 5 m wide pegmatitic syenogranite dyke, as well as a 10 m wide diabase dyke belonging to the Franklin dyke swarm (Fig. 17a). The psammite was selected for detrital zircon geochronology to provide constraints on its depositional age and identify detrital sources. The metasedimentary sequences in map sheet 38B have not been previously dated, and detrital zircon ages will provide new insights into how these rocks may correlate with the MRG further south, as well as with supracrustal rocks further afield.

Zircon crystals recovered from sample 17SAB-D126A2 were mostly clear and colourless to slightly turbid, subhedral, stubby to equant, with poorly-faceted to rounded edges (Fig. 17d-g). Rare elongate grains were also recovered. In BSE images, zircon interiors exhibit oscillatory zoning or display broad concentric, patchy or sector zoning (Fig. 17e-f). Many crystals have distinct rims or recrystallized zones that in some cases truncate zoning in grain interiors (Fig. 17g).

Seventy-three analyses were conducted across 61 zircon crystals, with $^{207}\text{Pb}/^{206}\text{Pb}$ ages between ca. 2961 and 2564 Ma (Fig. 17h; Appendix 1). Of these, one analysis was not considered in age calculations owing to high common Pb (3.78%; analysis 12276-087.1) although its $^{207}\text{Pb}/^{206}\text{Pb}$ age overlaps with the main cluster of analyses. Following the methodology outlined above (in “Methods” section), sixty $^{207}\text{Pb}/^{206}\text{Pb}$ ages from sample 17SAB-D126A2 were plotted in the program AgeDisplay (Sircombe, 2000). Of these, all were from grain interiors (no rim analyses), 52 were single-spot analyses (i.e., one analysis per zircon grain) and 8 were representative ages of zircon grains with multiple analyses. On a probability density distribution plot (Fig. 17i), the data display a dominant mode at 2720 Ma, as well as smaller ones at 2960-2940, 2880-2870, 2830, and 2770 Ma.

Additionally, four rim analyses (blue ellipses; Fig. 17h) from three different grains yielded a $^{207}\text{Pb}/^{206}\text{Pb}$ weighted average age of 2592 ± 11 Ma (MSWD=0.44, POF=0.73). As these analyses also had markedly low Th/U ratios (0.02-0.05) relative to other analyses in the sample, their age is considered to represent the timing of metamorphic zircon growth/recrystallization. Assuming this process was post-depositional, the psammite is interpreted to have undergone metamorphism at ca. 2592 Ma.

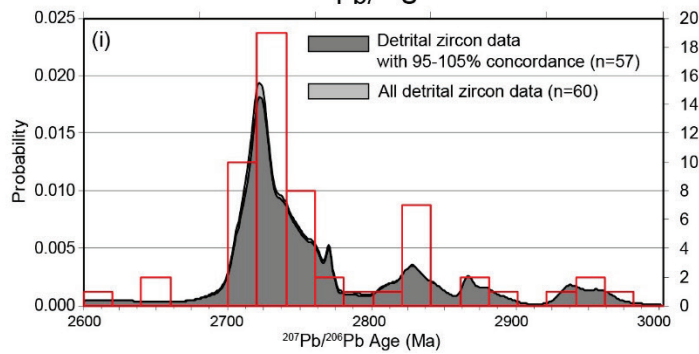
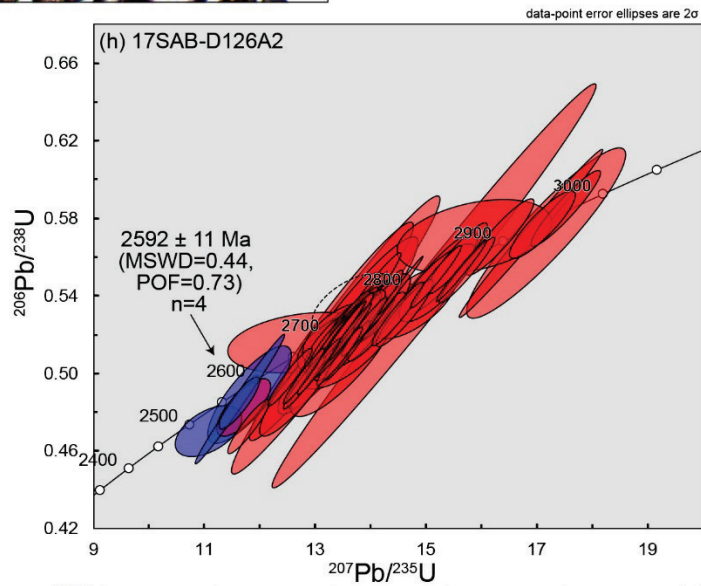
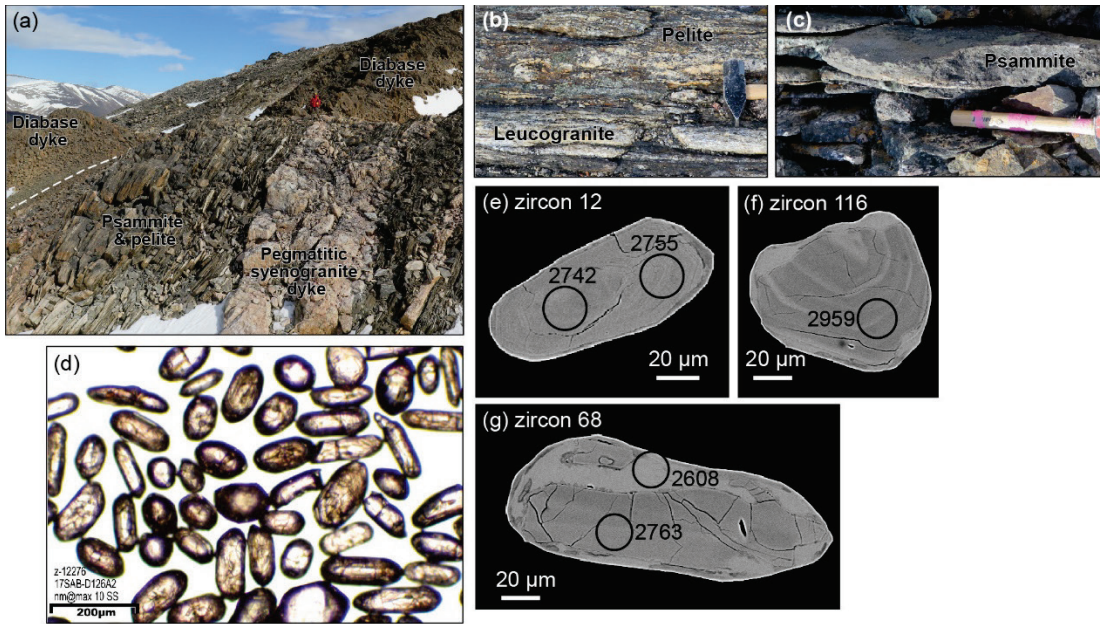


Fig. 17 (previous page): (a) Field photograph of interbedded pelite and psammite (dated by sample 17SAB-D126A2), cross-cut by a pegmatitic syenogranite dyke. These units are in turn cross-cut by a late diabase dyke belonging to the Franklin suite. Person for scale is 1.9 m tall. (b) Biotite-rich pelite with concordant bands of biotite-garnet leucogranite, which is interpreted as partial melt. Hammer head for scale is 8 cm long. (c) Photograph of the homogeneous psammite from which sample 17SAB-D126A2 was collected. Hammer handle for scale is 30 cm long. (d-g) Representative images of zircon recovered from the same sample, taken in transmitted light (d) and BSE mode (e-g). (h) Concordia plot showing SHRIMP U-Pb zircon data obtained from sample 17SAB-D126A2. The plot also presents the zircon rim age, as calculated from the data shown by blue ellipses. Red ellipses represent analyses that were considered in detrital age calculations. (i) Combined probability density and histogram diagram of detrital zircon $^{207}\text{Pb}/^{206}\text{Pb}$ ages from the same sample.

The maximum depositional age of the psammite is interpreted to be ca. 2720 Ma, the age of the youngest dominant mode on the probability density diagram. Uncommon younger analyses (i.e., ca. 2695-2615 Ma) are considered unreliable estimates of the maximum depositional age because: (i) some of the younger ages could not be reproduced by replicate analyses on the same grains, and (ii) the proximity of some of these analysis spots to grain edges suggest mixing with rim material. Therefore, the ca. 2695-2615 Ma zircon dates may represent partial resetting of older zircon during ca. 2592 Ma metamorphism.

17SAB-D073A4 (z12158): Biotite garnet cordierite psammite

Psammite in the Qimivviq area (Fig. 3a) is medium grained and composed of quartz, plagioclase, K-feldspar, biotite, and garnet, which forms 2-10 mm wide, round to lens-shaped porphyroblasts. Psammite also contains plagioclase porphyroblasts up to 1 cm in diameter. Foliation is defined by aligned biotite and compositional banding (Fig. 18a, b). Coarse-grained quartz, plagioclase, K-feldspar, and cordierite (\pm garnet) form 2-5 cm patches oriented parallel to foliation, which are interpreted as partial melts (Fig. 18b). Melt patches were avoided during sample collection and processing for zircon separation. The psammite forms part of a ~1 km thick sequence of interbedded pelite, semi-pelite, and psammite that dips shallowly toward the northeast, along a sharp contact with overlying tonalitic gneiss from which sample D218B1 was collected (described above; Fig. 9a, b). The psammite was collected for detrital zircon U-Pb geochronology to provide depositional age constraints and detrital source information for metasedimentary rocks in the Qimivviq area. Additionally, the age of the psammite has implications for whether its sharp contact with overlying tonalite gneiss might be a thrust fault, with an older-over-younger relationship.

Zircon crystals recovered from this sample mostly form 2-4:1 prisms with sub-rounded crystal faces, as well as less common stubby, oval-shaped grains (Fig. 18c). Zircon crystals are typically murky brown-coloured and fractured. Core-overgrowth relationships are apparent in several grains. In BSE (Fig. 18d-f), all zircon grains are fractured and pitted, and exhibit oscillatory to irregular zoning. The grains contain patchy or diffuse domains that truncate primary zoning, which likely represent zones of metamictization and/or recrystallization (Fig. 18d-f).

Twenty-five analyses in 21 grains yielded highly variable $^{207}\text{Pb}/^{206}\text{Pb}$ ages, ranging from ca. 3015 to 1497 Ma (Fig. 18g, h; Appendix 1). Although several analyses are near concordant (% discordance ≤ 5), most are

moderately to strongly discordant (7–31%). Many analyses have significantly elevated UO/U ratios (>7.3) relative to reference standards (6.3–6.9), which indicates a discrepancy between the matrices of the reference material and the unknowns and correlates strongly with the observed discordance. For these reasons, only a limited number of analyses were obtained from this sample and the majority of dates yielded are unrepresentative of detrital zircon sources. Only analyses with typical UO/U will be considered further.

Four analyses with ages of ca. 2518–2493 Ma cluster on Concordia (red ellipses; Fig. 18d) and yield a $^{207}\text{Pb}/^{206}\text{Pb}$ weighted average age of 2509 ± 19 Ma (MSWD=3.8, POF=0.01). These analyses are from distinct light-BSE domains (Fig. 18e, f), some of which truncate primary zoning (Fig. 18e), suggesting that they represent zones of recrystallization rather than detrital components. Some ca. 2509 Ma light-BSE domains yielded non-reproducible ages: one such domain (in grain #39) yielded two distinct ages of ca. 2516 and 1885 Ma (Fig. 18e), implying that 2509 Ma may not necessarily represent a distinct episode of zircon recrystallization. However, the ca. 2526–2491 Ma crystallization age of nearby leucogranite (sample 17SAB-D69B1, discussed above), which is interpreted as a partial melt of host metasedimentary strata, corroborates the existence of a ca. 2509 Ma thermal event that caused partial recrystallization of zircon in the psammite. Thus, grain 39 is considered to record two recrystallization events, at ca. 2509 and 1885 Ma. This interpretation is supported by the abundance and range of Paleoproterozoic ages from light-BSE recrystallized zones in the psammite sample, which suggests that detrital zircon underwent partial to complete recrystallization during and after ca. 2509 Ma. The timing of the later recrystallization event is estimated at ca. 1885 Ma, which is the age of a concordant analysis (with typical UO/U content) from a light-BSE recrystallized zone. A regression line through the 2518–2493 Ma analyses with a forced lower intercept of 1885 ± 20 Ma gave an upper intercept age of 2560 ± 41 Ma (MSWD=0.23). Thus, the older recrystallized zones are considered to record a thermal event with a maximum age of 2560 ± 41 Ma and a minimum age of ca. 2509 Ma.

Two analyses from zircon cores yielded $^{207}\text{Pb}/^{206}\text{Pb}$ ages that are older than the ca. 2560–2509 Ma recrystallization and, therefore, may provide a maximum depositional age for the psammite sample: 3015 ± 10 Ma (Fig. 18d) and 2698 ± 49 Ma (green ellipses; Fig. 18g, h). As the 2698 ± 49 Ma analysis is discordant (16%) and has a high common Pb content (4.87%), it is considered to represent a minimum estimate of the maximum depositional age. The minimum depositional age is provided by the ca. 2560–2509 Ma age of zircon recrystallization.

17SAB-E122A1 (z12278): Muscovite chlorite quartzite

This quartzite was mapped as part of the MRG in the Tuktularvik area (Fig. 3). It is medium grained, blue-grey in colour (Fig. 19a), and contains muscovite, chlorite, and minor feldspar. Aligned micas define a weak foliation, and the quartzite is characterized by a strong stretching lineation. The quartzite has a sharp, locally irregular contact with the monzogranite from which sample 17SAB-E122B1 was collected (described above; Fig. 8a). The quartzite was sampled for detrital zircon U-Pb geochronology to provide depositional age constraints and detrital source information for the MRG.

Most zircon grains recovered from this sample form stubby (1.5–2:1 aspect ratio) to equant crystals that range in appearance from clear and colourless to cloudy/fractured and pale brown (Fig. 19b). The sample also contains a sub-population of larger, more elongate prismatic zircon crystals that are brown in colour and contain numerous fractures. Regardless of morphology, the zircon grains are typically subhedral, with irregular ‘bumpy’-textured edges that may be attributed to sedimentary transport (Fig. 19c–f). They exhibit a variety of internal zoning patterns in BSE, including fine to broad oscillatory zoning and patchy,

irregular or sector zoning (Fig. 19c-f). Some grains comprise a patchy, zoned core enclosed by a rim with fine oscillatory zoning (Fig. 19e, f).

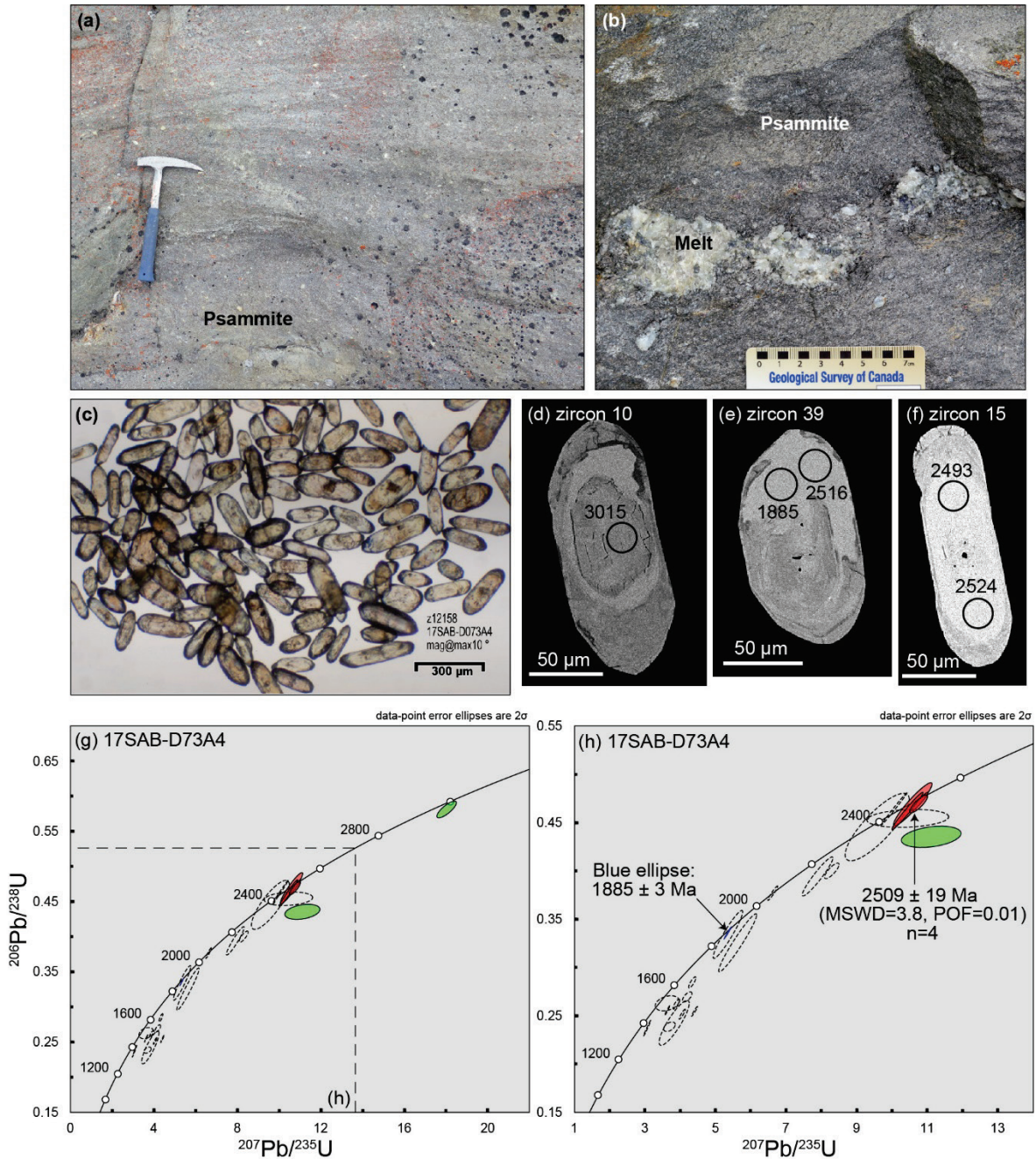


Fig. 18: (a) Field photograph of psammite from which sample 17SAB-D73A4 was collected. Hammer for scale is 32 cm long. (b) Field photograph of a cordierite-bearing melt patch in psammite. (c-f) Representative images of zircon recovered from sample 17SAB-D73A4, taken in transmitted light (c) and BSE mode (d-f). (g, h) Concordia diagrams showing SHRIMP U-Pb zircon data for the same sample.

Seventy-one analyses from 60 zircon grains yielded $^{207}\text{Pb}/^{206}\text{Pb}$ ages ranging from ca. 3145 to 2485 Ma (Fig. 19g; Appendix 1). Sixty $^{207}\text{Pb}/^{206}\text{Pb}$ ages from sample 17SAB-E122A1 were plotted in AgeDisplay (Sircombe, 2000), including 50 single-spot analyses (i.e., one analysis per zircon grain) and 10 representative ages of zircon grains with multiple analyses. On a combined probability density and histogram diagram (Fig. 19h), the data display a dominant mode at 2705 Ma, as well as smaller ones at 3145, 2915, 2680, and 2660 Ma. Whether the youngest clusters of ages at ca. 2680-2660 Ma reflect Pb loss from >2700 Ma grains or represent the maximum depositional age of quartzite sample 17SAB-E122A1 is difficult to assess with the present data. Therefore, the dominant zircon population at ca. 2705 Ma is interpreted as a conservative estimate of the maximum age of deposition of the quartzite.

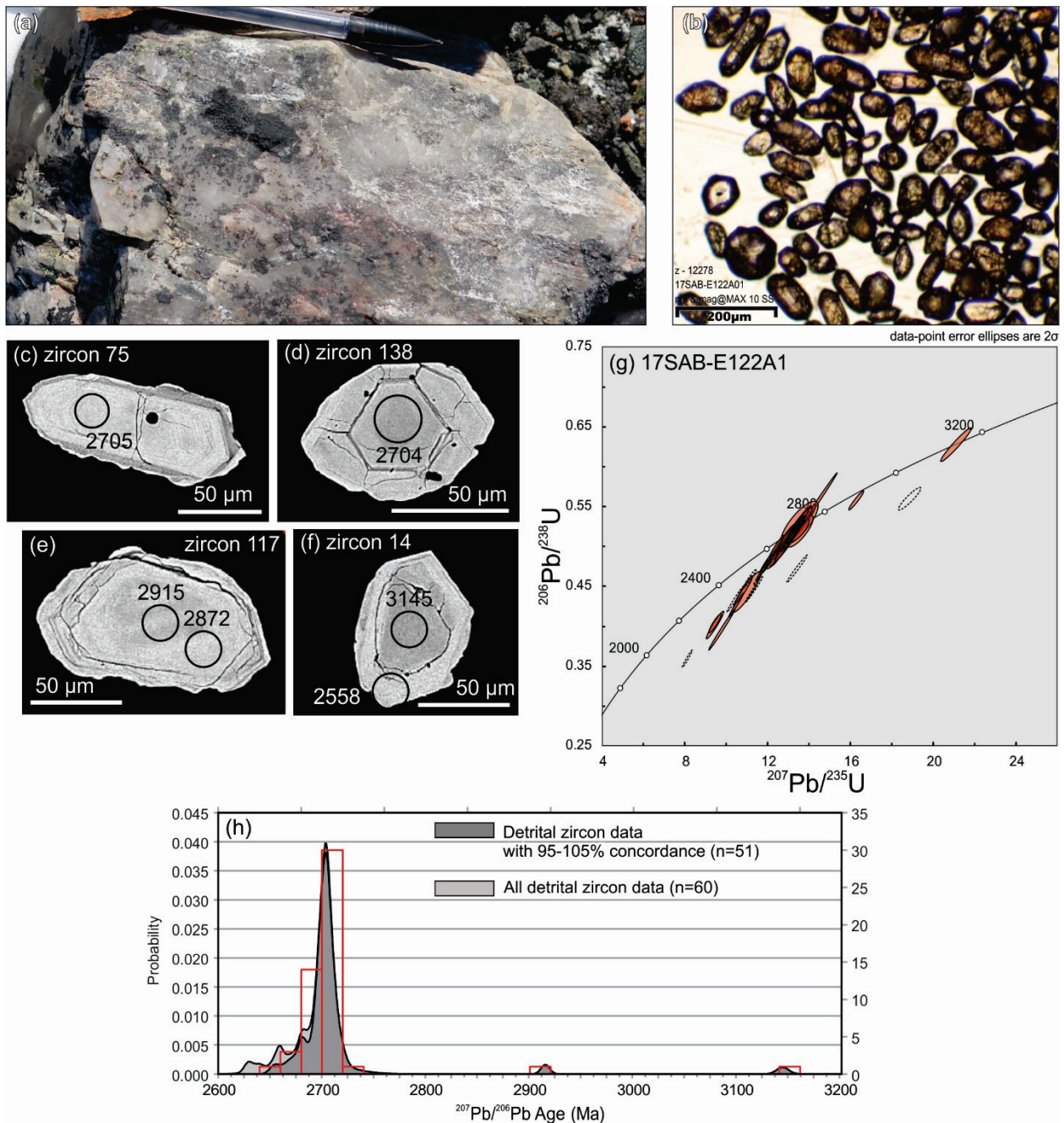


Fig. 19 (previous page): (a) Field photograph of quartzite in the Tuktuliarvik area, from which sample 17SAB-E122A1 was collected. Pencil for scale. (b-f) Representative images of zircon recovered from the same sample, in transmitted light (b) and BSE mode (c-f). (g) Concordia diagram showing SHRIMP U-Pb zircon isotopic data for sample 17SAB-E122A1. Red ellipses represent analyses that were considered in detrital age calculations (dashed ellipses are replicate analyses excluded from the combined plot in (h)). (h) Combined probability density and histogram plot of detrital zircon $^{207}\text{Pb}/^{206}\text{Pb}$ ages from the same sample.

Summary and Conclusions

Basement orthogneiss

The oldest rocks dated in the study area are granodiorite (ca. 2901 Ma) underlying the MRG at Deposit 4 and quartz diorite gneiss (ca. 2892 Ma) along Oliver Sound (Fig. 3a). They are somewhat older than the ca. 2851 Ma tonalite gneiss, dated and mapped as the basement to the MRG by Jackson et al. (1990), and the ca. >2843 Ma tonalite-granodiorite cobble from Ege Bay (Bethune and Scammell, 2003a). Therefore, together with younger ca. 2780–2775 Ma gneissic rocks from the Ege Bay area, the age of gneissic basement underlying the MRG is estimated to be ca. 2901–2775 Ma. Ca. 3555–3400 and 2921 Ma inherited zircon in monzogranite (17SAB-E122B1) and granodiorite (03-NB-4134), respectively, suggests older, deeper crust, as supported by ca. 3000 Ma inherited zircon at Ege Bay (Bethune and Scammell, 2003a).

As the northern Rae craton in Canada and West Greenland is composed of mainly ca. 2.99–2.77 Ga felsic orthogneiss, the results presented herein are consistent with previous models that include northern Baffin Island as part of the Rae craton (e.g., St-Onge et al., 2009; Sanborn-Barrie et al., 2017).

Mary River Group and other supracrustal rocks

Meta-rhyolite (17SAB-E119A2) and meta-dacite (03-NB-4043) from the MRG in the Tuktuliarvik (Long Lake) area yielded ages of ca. 2833 and 2829 Ma, respectively. Detrital zircon from quartzite (17SAB-E122A1) in this same area defined a maximum depositional age of ca. 2705 Ma, in contrast to the structurally-higher ca. 2830 Ma volcanic units located a few kilometres away. Detailed geological mapping of this area suggests that the < ca. 2705 Ma quartzite and ca. 2830 Ma volcanic rocks were juxtaposed through complex fold-and-thrust relationships (Bros and Johnston, 2017; Bros, 2018).

Detrital zircon ages and morphologies suggest a local source for the < ca. 2705 Ma Tuktuliarvik quartzite, such as ca. 2731–2706 Ma plutonic and volcanic rocks (discussed below). The quartzite overlies monzogranite (17SAB-E122B1), which is dated herein at 2716 ± 4 Ma, along a sharp contact (Fig. 8a) that locally exhibits folding and interleaving. The geochronological data permit a depositional contact between the two units, which has been structurally reworked.

Further south, MRG dacite samples from east of the Mary River iron mine produced considerably younger ages of ca. 2731 Ma (03-NB-4048) and ca. 2718 Ma (Jackson et al., 1990) compared to the volcanic rocks at Tuktuliarvik, but similar to the timing of MRG volcanism at Ege Bay (ca. 2760–2725 Ma; Bethune and Scammell, 2003a). However, ca. 2814 Ma inherited zircon in monzogranite (17SAB-D173A1), with a possible source from adjacent amphibolite (Fig. 6a), provides indirect evidence for volcanism of that age east of the Mary River iron mine.

These new data suggest that MRG volcanism persisted from ca. 2830 to 2718 Ma or, alternatively, that there were two distinct episodes of volcanism at ca. 2830 (to 2814?) Ma and ca. 2760–2718 Ma, separated

by a ca. 70-110 Myr hiatus. The latter interpretation is preferred here because there are no known intervening dates. In turn, data from the quartzite at Tuktularvik suggest that < ca. 2705 Ma siliciclastic sedimentation postdated the younger phase of MRG volcanism by at least ca. 10 Myr and was unrelated to the ca. 2830 Ma volcanism at Tuktularvik. The proximity of the younger, ca. 2730-2720 Ma volcanic rocks to high-grade banded iron formation, including the Mary River iron mine, suggests that volcanic successions of this age are more prospective for hosting economic iron deposits than those dated at ca. 2830 Ma. This is supported by the similarly aged chlorite-garnet schist that has been dated in the Mary River mine ore zone (ca. 2748 ± 11 Ma; Fulcher, 2015).

Metasedimentary strata southeast of Pond Inlet (17SAB-D126A2) were deposited after ca. 2720 Ma. The minimum depositional age is provided by ca. 2592 Ma metamorphic zircon rims, assuming the rims formed after deposition. Although little detrital age information was extractable from psammite at Qimivviq (17SAB-D73A4), the metasedimentary strata from that area are lithologically equivalent to the psammite, semi-pelite, and pelite located southeast of Pond Inlet, which are also the closest meta-supracrustal rocks. At Qimivviq, deposition is loosely constrained between a maximum age of ca. 3015–2698 Ma and a minimum age of 2.56-2.50 Ga. The latter encapsulates the age of recrystallized zircon in the dated psammite (ca. 2560-2509 Ma) and that of partial melting (leucogranite 17SAB-D69B1; ca. 2526–2491 Ma). Therefore, it may be reasonably assumed that the metasedimentary strata at Qimivviq and southeast of Pond Inlet were both deposited after ca. 2720 Ma and prior to ca. 2.50 Ga. Considering the detrital zircon depositional ages obtained from metasedimentary rocks in the northern portion of the study area, it is possible that they were deposited synchronously with the younger, ca. 2720–post ca. 2705 Ma MRG further south. Together, they may record an Archean lateral stratigraphic transition from dominantly volcanic- and BIF-rich strata (MRG) to siliciclastic sequences (at Qimivviq and southeast of Pond Inlet), but more work would be required to test this hypothesis.

Field relationships at Qimivviq indicate that the metasedimentary rocks are in thrust contact with overlying tonalite gneiss (Skipton et al., 2017). However, the age data presented herein do not allow us to determine whether the original relationship between the 2706 ± 3 Ma tonalite gneiss and the post-ca. 3015–2698 Ma psammite was intrusive or depositional. Therefore, the contact between the two units (Fig. 9c) may be interpreted as a tectonically reworked intrusive or (overturned) depositional contact, or, alternatively, as a thrust that juxtaposed tonalite over psammite that it was not previously in contact with.

The MRG and other supracrustal rocks on northern Baffin Island show age and lithological similarities with greenstone belts to the southwest in the Rae craton, including the Committee Bay and Roche Bay belts (Fig. 1). For instance, the Committee Bay belt is composed of a ca. 2.73–2.68 Ga volcano-sedimentary complex that includes mafic–intermediate volcanic rocks, iron formation, komatiitic volcanic rocks, and a < ca. 2.69 Ga clastic ± komatiite sequence (Sanborn-Barrie et al., 2014). On Melville Peninsula, the lithologically similar Roche Bay belt records subvolcanic magmatism at ca. 2.765–2.760 Ga and at 2.72 Ga (Wodicka et al., 2011; Corrigan et al., 2013), as well as siliciclastic sedimentation with a maximum depositional age of ca. 2.72 Ga (N. Wodicka, unpubl. data). The MRG also demonstrates age and lithological similarities with the siliciclastic strata, ironstone, mafic volcanic and ultramafic rocks of the ca. 2.7–2.6 Ga (Rb-Sr and U-Pb ages; Dawes et al., 1988) Lauge Koch Kyst belt in the Rae craton on northern West Greenland (Dawes, 2006). Together with previous data, the new U-Pb ages for the MRG presented herein indicate that volcanism, siliciclastic sedimentation, and BIF deposition occurred in stages between ca. 2.765 and 2.6 Ga along a ~1000 km-long swath of the Rae craton, from the present-day Committee Bay area to West Greenland.

The ca. 2830 Ma volcanism in the MRG at Tuktularvik seems to be unique in age among the greenstone belts in the Rae craton. The known ages of the Committee Bay, Roche Bay, and Lauge Koch Kyst belts are

considerably younger, whereas the Prince Albert greenstone belt (ca. 2970 Ma; Wodicka et al., 2011) on Melville Peninsula is significantly older.

Felsic plutonic rocks

U-Pb data from plutonic rocks define an extensive ca. 2731-2706 Ma felsic plutonic suite, composed of foliated to massive monzogranite and granodiorite and, less commonly, gneissic tonalite. The emplacement of the felsic plutonic suite somewhat overlaps in age with the younger volcanic phase of the MRG, but mostly outlasts it. This is supported by field evidence of monzogranite and granodiorite intruding MRG volcanic rocks (Skipton et al., 2017). MRG volcanism was also outlasted by plutonism south of the study area at Ege Bay (ca. 2730–2715 Ma; Bethune and Scammell, 2003a). Post-ca. 2705 Ma siliciclastic sedimentation at Tuktuliarvik was either broadly contemporaneous with or postdated emplacement of the youngest felsic plutonic rocks of the 2731-2706 Ma suite.

As ca. 2.75–2.70 Ga felsic plutonism is widespread elsewhere in the northern Rae craton (e.g., Sanborn-Barrie et al., 2014), coeval plutonism on northern Baffin Island further supports a Rae cratonic affinity. However, no plutonic ages have yet been found on northern Baffin Island that are equivalent to the voluminous ca. 2.62-2.58 Ga Snow Island suite (e.g., Peterson et al., 2015) that extends across large portions of the central and southern portions of the Rae craton.

Mafic plutonic rocks

Mafic plutonic rocks near Pond Inlet, including gabbro (17SAB-D232A1) and a layered mafic-ultramafic intrusion (17SAB-B71A2), yielded ages of ca. <2720>2655 Ma and 2669 Ma, respectively. These mafic intrusions may have postdated emplacement of the ca. 2731–2706 Ma felsic plutonic rocks described above by ca. 35-50 Ma.

Timing of metamorphism and deformation

Zircon ages and field relationships provide insights into the timing of metamorphism and deformation. In ca. 2892 Ma quartz diorite (17SAB-D10D1), ca. 2709 Ma zircon domains probably reflect thermal overprinting by felsic intrusions of that age. This is supported by field relationships indicating that quartz diorite is the oldest component of the gneiss complex at this locality; it was intruded by granodiorite and monzogranite layers/veins. Cross-cutting relationships between the plagioclase-phyric granodiorite sill (03-NB-4049) east of the Mary River iron mine and host mafic-to-intermediate metavolcanic rocks of the MRG suggest that foliation development in the MRG predated, at least in part, ca. 2726 Ma, and that the strong lineation in the sill formed either synchronously with or after emplacement of the ca. 2726 Ma sill.

As outlined above, evidence of ca. 2.60-2.50 Ga metamorphism is recorded locally in the northern portion of the study area. In psammite southeast of Pond Inlet (17SAB-D126A2), low-Th/U zircon domains suggest post-depositional metamorphic overprinting at ca. 2592 Ma. At Qimivviq, crystallization of leucogranite (17SAB-D69B1) interpreted as a partial melt of metasedimentary host rocks is bracketed between ca. 2526 and 2491 Ma. Recrystallized zones in zircon from the nearby psammite (17SAB-D73A4) suggest a thermal event at ca. 2560–2509 Ma, likely related to partial melting. A preliminary zircon date of ca. 2540 Ma from the charnockitic Bylot batholith (D.J. Scott and G.D. Jackson, unpublished U-Pb SHRIMP data; Jackson and Berman, 2000) suggests that late Neoproterozoic thermal activity in the northern part of the study area followed (or accompanied?) Bylot batholith emplacement. However, it must be noted that no other known U-Pb dates exist for the Bylot batholith, and it is uncertain whether the ca. 2540 Ma zircon represents igneous crystallization or a later metamorphic overprint.

Ca. 2.60–2.50 Ga metamorphism on northern Baffin Island is similar in age, at least in part, to ca. 2.54–2.34 Ga metamorphism and deformation that has been documented in the Rae craton from the southern Northwest Territories to Melville Peninsula, and has been attributed to the Arrowsmith orogen (Berman et al., 2013). Therefore, new evidence of ca. 2.60–2.50 Ga metamorphism presented here may indicate that the Arrowsmith orogen extended further northeastward onto northern Baffin Island, as has been previously proposed (Berman et al., 2013). Additional research is needed to investigate this theory.

Several samples record Paleoproterozoic regional metamorphism. Low-Th/U zircon rims and crystals in mafic plutonic rocks near Pond Inlet (17SAB-D232A1, -B71A2) range in age from ca. 1926 to 1892 Ma. Zircon rims in monzogranite at Tuktuliarvik (17SAB-E122B1) were dated at ca. 1878 Ma, similar to the recrystallization age of zircon in psammite at Qimivviq (17SAB-D73A4) estimated at ca. 1885 Ma. These data suggest that the study area, or at least the area spanning Tuktuliarvik, Qimivviq, and Oliver Sound, was affected by regional metamorphism from ca. 1926 to 1878 Ma. South of the study area, at Ege Bay, Bethune and Scammell (2003b) reported younger Paleoproterozoic tectono-metamorphism spanning ca. 1850 to 1820 Ma (based on U-Pb zircon, monazite, titanite dates). Together, the data imply that northern Baffin Island was affected by several regional metamorphic events during a ca. 100 Myr period in the middle Paleoproterozoic, and that metamorphism may have occurred later (or was longer-lived) in the Steensby Inlet – Barnes Ice Cap area than further north in the Pond Inlet – Tuktuliarvik area.

The youngest rock dated in this study is a syenogranite pluton (17SAB-B98A1) that cross-cuts foliation in tonalite gneiss south of Pond Inlet. The crystallization age of the syenogranite, ca. 1792 Ma, provides a lower age limit on regional deformation.

Possible causes of regional metamorphism (and coeval deformation) on northern Baffin Island between ca. 1926 and 1820 Ma include orogenic events that have previously been documented elsewhere in the Rae craton, on southern Baffin Island, and/or in Greenland. For example, tectono-metamorphism during ca. 1850–1820 Ma at Ege Bay has been attributed to an early phase of the Trans-Hudson orogen (Bethune and Scammell, 2003b). Similarly, ca. 1.85–1.82 Ga tectono-metamorphism in the Committee Bay belt has been attributed to microcontinent collisions along the southeastern margin of the Rae craton during an early stage of the Trans-Hudson orogen (Sanborn-Barrie et al., 2013). Older (ca. 1926–1878 Ma) tectono-metamorphism on northern Baffin Island could possibly have been produced during the ca. 1.96–1.92 Ga Ellesmere-Inglefield orogen, which outlines the northern margin of the Rae craton in Arctic Canada (between Baffin and Devon islands) and West Greenland (St-Onge et al., 2009). Additional work is required to investigate the tectono-metamorphic history of northern Baffin Island and potential links with orogenic activity in the region.

Future Geochronological Work

Additional samples were collected for U-Pb zircon geochronology in the Steensby Inlet – Barnes Ice Cap area during fieldwork in 2018 (Saumur et al., 2018c; Skipton et al., 2018b). U-Pb zircon geochronology is planned on approximately 13 samples to determine crystallization ages of felsic gneiss and intrusive suites, as well as depositional ages of the Mary River and Piling groups. Additional samples from the 2017 field area will also be dated, including garnet-bearing monzogranite from Pond Inlet. U-Pb monazite dating of regionally distributed supracrustal rocks is in progress, with the aim of elucidating the regional metamorphic and structural evolution.

Acknowledgements

This work was financially supported by the GSC GEM-2 North Baffin project (2017-2020) and by the Canada-Nunavut Geoscience Office and GSC's North Baffin study (2002-2005). DRS was supported by the GSC's Alice Wilson Postdoctoral Fellowship. The authors thank Annick Morin, Erin Bros, Mick Appaqaq, Tyler Rowe, Owen Weller and Stephen Johnston for their insights and their assistance in collecting geochronology samples. Pamela Iraheta Muniz and Sean Hicks are thanked for their help in preparing grain mounts. The authors are grateful to Pat Hunt and Meghan Moher for acquiring SEM images, and to Bill Davis, Tom Pestaj, Nicole Rayner and Daniele Regis for their insights and help in the SHRIMP lab. Nicole Rayner is thanked for her critical review that improved the quality of this manuscript.

References

- Berman, R.G., Pehrsson, S., Davis, W.J., Ryan, J.J., Qui, H., Ashton, K.E., 2013. The Arrowsmith Orogeny: geochronological and thermobarometric constraints on its extent and tectonic setting in the Rae craton, with implications for pre-Nuna supercontinent reconstruction. *Precambrian Research* 232, 44–69.
- Bethune, K.M. and Scammell, R.J. 2003a. Geology, geochronology, and geochemistry of Archean rocks in the Ege Bay area, north-central Baffin Island, Canada: constraints on the depositional and tectonic history of the Mary River Group of northeastern Rae Province. *Canadian Journal of Earth Sciences* 40, 1137–1167.
- Bethune, K.M. and Scammell, R.J. 2003b. Distinguishing between Archean and Paleoproterozoic tectonism, and evolution of the Isortoq fault zone, Ege Bay area, north-central Baffin Island, Canada. *Canadian Journal of Earth Sciences* 40, 1111–1135.
- Bros, E.R., Johnston, S.T., 2017. Field observations of the Mary River Group south of Tay Sound, northern Baffin Island, Nunavut: stratigraphy and structure of supracrustal sequences and surrounding plutonic units; in *Summary of Activities 2017*, Canada-Nunavut Geoscience Office, 69–80.
- Bros, E.R., 2018. Observations of the Mary River Group south of Tay Sound, northern Baffin Island, Nunavut: stratigraphy and structure of a supracrustal sequence. *Nunavut Mining Symposium 2018*, Iqaluit, Nunavut. <https://www.nunavutminingsymposium.ca/2018>
- Corrigan, D., Pehrsson, S., Wodicka, N. and de Kemp, E., 2009. The Palaeoproterozoic Trans-Hudson Orogen: a prototype of modern accretionary processes. *Geological Society, London, Special Publications* 2009, 327, 457–479. doi: 10.1144/SP327.19
- Corrigan, D., Nadeau, L., Brouillette, P., Wodicka, N., Houlié, M.G., Tremblay, T., Machado, G., and Keating, P., 2013. Overview of the GEM Multiple Metals - Melville Peninsula project, central Melville Peninsula, Nunavut. *Geological Survey of Canada, Current Research no. 2013-19*, 21 p. doi:10.4095/292862
- Davidson, A., Jackson, G.D. and Morgan, W.C. 1979. *Geology, Icebound Lake, District of Franklin*; Geological Survey of Canada, Map 1451A, coloured, with expanded legend, scale 1:250 000. <https://doi.org/10.4095/109161>
- Dawes, P.R., 2006. Explanatory notes to the Geological map of Greenland, 1:500 000, Thule, Sheet 5. *Geological Survey of Denmark and Greenland Map Series* 2, 97 pp.
- Dawes, P.R., Larsen, O., Kalsbeek, F., 1988. Archean and Proterozoic crust in North-West Greenland: Evidence from Rb-Sr whole-rock age determinations. *Canadian Journal of Earth Sciences* 25, 1365–1373.
- de Kemp, E.A. and Scott, D.J., 1998. *Geoscience compilation of the Northern Baffin Island and Northern Melville Peninsula, Northwest Territories*. Geological Survey of Canada, Open File D3636.

- Fulcher, S.A., 2015. The Lithotectonic Setting and Paragenetic History of Deposit No. 1, Mary River District, North Baffin Island. Electronic Thesis and Dissertation Repository. 2884.
<https://ir.lib.uwo.ca/etd/2884>
- Jackson, G.D., Hunt, P.A., Loveridge, W.D. and Parrish, R.R. 1990. Reconnaissance geochronology of Baffin Island, N.W.T.; in Radiogenic Age and Isotopic Studies: Report 3, Geological Survey of Canada Paper 89-2, 123–148.
- Jackson, G.D. and Davidson, A. 1975. Geology, Pond Inlet and Nova Zembla Island, District of Franklin; Geological Survey of Canada, Map 1396A, coloured, with expanded legend, scale 1:250 000.
<https://doi.org/10.4095/109005>
- Jackson, G.D. and Morgan, W.C. 1978. Geology, Conn Lake, District of Franklin; Geological Survey of Canada, Map 1458A, coloured, with expanded legend, scale 1:250 000.
<https://doi.org/10.4095/109162>
- Jackson, G.D., Morgan, W.C. and Davidson, A. 1978. Geology, Steensby Inlet, District of Franklin; Geological Survey of Canada, Map 1450A, coloured, with expanded legend, scale 1:250 000.
<https://doi.org/10.4095/109160>
- Jackson, G.D. 2000. Geology of the Clyde-Cockburn Land map area, north-central Baffin Island, Nunavut; Geological Survey of Canada, Memoir 440, 316 pp.
- Jackson, G.D. and Berman, R.G. 2000. Precambrian metamorphic and tectonic evolution of northern Baffin Island, Nunavut, Canada. *The Canadian Mineralogist* 38, 399–421.
- Johns, S.M. and Young, M.D., 2006. Bedrock geology and economic potential of the Archean Mary River group, northern Baffin Island, Nunavut; Geological Survey of Canada Current Research 2006-C5, 13 p.
- Krogh, T.E., 1982. Improved accuracy of U-Pb zircon ages by the creation of more concordant systems using an air abrasion technique; *Geochimica et Cosmochimica Acta*, v. 46, p. 637-649.
- LaFlamme, C., McFarlane, C.R.M. and Corrigan, D. 2014. U-Pb, Lu-Hf and REE in zircon from 3.2 to 2.6 Ga Archean gneisses of the Repulse Bay block, Melville Peninsula, Nunavut. *Precambrian Research* 252, 223–239.
- Leshner, C.M. 2007: Ni-Cu-(PGE) deposits in the Raglan area, Cape Smith Belt, New Quebec; in *Mineral Deposits of Canada: a Synthesis of Major Deposit Types, District Metallogeny, the Evolution of Geological Provinces and Exploration Methods*, W.D. Goodfellow (ed.), Geological Association of Canada, Special Publication, v. 5, p. 351–386.
- Ludwig, K.R., 2009. Isoplot 4.1, A geochronological toolkit for Microsoft Excel. Berkeley Geochronology Center Special Publication 4, 76 p.
- Parrish, R.R., Roddick, J.C., Loveridge, W.D., and Sullivan, R.W., 1987. Uranium-lead analytical techniques at the Geochronology Laboratory, Geological Survey of Canada; in *Radiogenic age and isotopic studies, Report 1*; Geological Survey of Canada, Paper 87-2, p. 3-7. Pehrsson, S., Jefferson, C., Corrigan, D., Sanborn-Barrie, M., Berman, R. and Peterson, T., 2011. Unravelling the mineral potential of the Churchill province. In: *Prospector's and Developer's Association of Canada, Annual Convention (PDAC)*. CD-ROM.
- Pehrsson, S.J., Berman, R.G., Eglinton, B. and Rainbird, R., 2013. Two Neoarchean supercontinents revisited: The case for a Rae family of cratons; *Precambrian Research* 232, 27-43.
- Peterson, T.D., Jefferson, C.W., and Anand, A., 2015. Geological setting and geochemistry of the ca. 2.6 Ga Snow Island Suite in the central Rae Domain of the Western Churchill Province, Nunavut; Geological Survey of Canada, Open File 7841, 29 p. doi:10.4095/296599
- Roddick, J.C., 1987. Generalized numerical error analysis with applications to geochronology and thermodynamics; *Geochimica et Cosmochimica Acta*, v. 51, p. 2129-2135.

- Sanborn-Barrie, M., Davis, W.J., Berman, R.G., Rayner, N., Skulski, T. and Sandeman, H. 2014. Neoproterozoic continental crust formation and Paleoproterozoic deformation of the central Rae craton, Committee Bay belt, Nunavut; *Canadian Journal of Earth Sciences* 51, 635–667.
- Saumur, B.M., Skipton, D.R., St-Onge, M.R., Wodicka, N., Bros, E.R. and Weller, O.M., 2018a. Bedrock geology, Mumiksa-Milne Inlet, Nunavut, parts of NTS 38-B and 48-A. Geological Survey of Canada, Canadian Geoscience Map 348, scale 1:100 000, 1 sheet.
- Saumur, B.M., Skipton, D.R., St-Onge, M.R., Wodicka, N., Bros, E.R. and Weller, O.M., 2018b. Bedrock geology, Kanajuqtuuq (Paquet Bay), Nunavut, NTS 37-G north. Geological Survey of Canada, Canadian Geoscience Map 349, scale 1:100 000, 1 sheet.
- Saumur, B.M., Skipton, D.R., St-Onge, M.R., Bros, E.R., Acosta-Gongora, P., Kelly, C.J., Morin, A., O'Brien, M.E., Johnston, S.T. and Weller, O.M., 2018c. Precambrian geology of the surroundings of Steensby Inlet and western Barnes Ice Cap (parts of NTS37E, 37F, 37G), Baffin Island, Nunavut; in *Summary of Activities 2018, Canada-Nunavut Geoscience Office*, p. 29–46.
- Sircombe, K., 2000. The usefulness and limitations of binned frequency histograms and probability density distributions for displaying absolute age data. Geological Survey of Canada, *Radiogenic Age and Isotopic Studies: Report 13, Current Research 2000-F2*, 11 p.
- Skipton, D.R., Saumur, B.M., St-Onge, M.R., Wodicka, N., Bros, E.R., Morin, A., Brouillette, P., Weller, O.M. and Johnston, S.T., 2017. Precambrian bedrock geology of the Pond Inlet–Mary River area, northern Baffin Island, Nunavut; in *Summary of Activities 2017, Canada-Nunavut Geoscience Office*, 49–68.
- Skipton, D.R., Saumur, B.M., St-Onge, M.R., Wodicka, N., Bros, E.R., Currie, L.D., Haggart, J.W. and Weller, O.M., 2018a. Bedrock geology, Pond Inlet, Nunavut, part of NTS 38-B. Geological Survey of Canada, Canadian Geoscience Map 347, scale 1:100 000, 1 sheet.
- Skipton, D.R., Saumur, B.M., St-Onge, M.R., 2018b. Report of Activities for the GEM-2 Baffin Project (2018): regional bedrock mapping of northern Baffin Island (Steensby Inlet and Barnes Ice Cap areas), Nunavut. Geological Survey of Canada, Open File 8484, 16 p.
- Snyder, D.B., Berman, R.G., Kendall, J-M. and Sanborn-Barrie, M. 2013. Seismic anisotropy and mantle structure of the Rae craton, central Canada, from joint interpretation of SKS splitting and receiver functions. *Precambrian Research* 232, 189–208. doi:10.1016/j.precamres.2012.03.003.
- Spratt, J.E., Skulski, T., Craven, J.A., Jones, A.G., Snyder, D.B. and Kiyani, D. 2014. Magnetotelluric investigations of the lithosphere beneath the central Rae craton, mainland Nunavut, Canada; *Journal of Geophysical Research: Solid Earth* 119, 2415–2439. doi:10.1002/2013JB010221.
- Steiger, R. H., and Jäger, E., 1977. Subcommission on geochronology; Convention on the use of decay constants in geo- and cosmochronology. *Earth and Planetary Science Letters* 36, 359–362.
- St-Onge, M.R., Searle, M.P., Wodicka, N., 2006. Trans-Hudson Orogen of North America and Himalaya-Karakoram-Tibetan Orogen of Asia: Structural and thermal characteristics of the lower and upper plates. *Tectonics* 25, 1–22.
- St-Onge, M.R., van Gool, J.A.M., Garde, A.A., Scott, D.J., 2009. Correlation of Archaean and Paleoproterozoic units between northeastern Canada and western Greenland: constraining the pre-collisional upper plate accretionary history of the Trans-Hudson Orogen. *Journal of the Geological Society, London* 318:193–235. <http://dx.doi.org/10.1144/SP318.7>.
- St-Onge, M.R., Scott, D.J., Rayner, N., Sanborn-Barrie, M., Skipton, D.R., Saumur, B.M., Wodicka, N. and Weller, O.M., 2020. Archean and Paleoproterozoic cratonic rocks of Baffin Island; in Dafoe, L. and Bingham-Koslowski, N. (eds), *Baffin Geological Synthesis*, Geological Survey of Canada, Bulletin xxx.
- Stern, R.A., 1997. The GSC Sensitive High Resolution Ion Microprobe (SHRIMP): Analytical Techniques of Zircon U–Th–Pb Age Determinations and Performance Evaluation. *Radiogenic Age and Isotopic Studies, Report 10*. Geological Survey of Canada, *Current Research 1997-F*, 1–31.

- Stern, R.A., Amelin, Y., 2003. Assessment of errors in SIMS zircon U–Pb geochronology using a natural zircon standard and NIST SRM 610 glass. *Chemical Geology* 197, 111–146.
- Turner, E.C., 2009. Mesoproterozoic carbonate systems in the Borden Basin, Nunavut. *Canadian Journal of Earth Sciences* 46, 915–938.
- Turner, E.C., 2011. Structural and stratigraphic controls on carbonate-hosted base metal mineralization in the Mesoproterozoic Borden Basin (Nanisivik District), Nunavut. *Economic Geology* 106, 1197–1223.
- White, L. and Ireland, T., 2012. High-uranium matrix effect in zircon and its implications for SHRIMP U-Pb age determinations. *Chemical Geology* 306-307, 78-91.
- Wodicka, N., Corrigan, D., Nadeau, L., and Erdmann, S., 2011. New U-Pb geochronological results from Melville Peninsula: Unravelling the Archean and early Paleoproterozoic magmatic history of the north-central Rae craton, in Geological Association of Canada–Mineralogical Association of Canada Annual Meeting, Ottawa, Abstracts Volume 34, p. 236.
- Young, M.D., Sandeman, H., Berniolles, F. and Gertzbein, P.M., 2004. A preliminary stratigraphic and structural geology framework of the Archean Mary River Group, northern Baffin Island, Nunavut; Geological Survey of Canada, Current Research 2004-C1, 14 p.
- Young M., McNicoll, V., Sandeman H., Creaser R., Johns, S., James D., 2007. Meso- to Neoproterozoic crustal growth and recycling on northern Baffin Island and correlation of Rae Province rocks across mainland Nunavut and Greenland, in Geological Association of Canada–Mineralogical Association of Canada Annual Meeting, Yellowknife, Abstracts Volume 32, p. 89.
- Zhang, S. 2018. Ordovician stratigraphy on the unnamed peninsula (southwestern NTS area 37F and northwestern NTS area 37C) northeast of Fury and Hecla Strait on northern Baffin Island, Nunavut; *in* Summary of Activities 2018, Canada-Nunavut Geoscience Office, 97–106.